Available online at www.sciencedirect.com
SCIENCE DIRECT
Earth-Science Reviews 77 (2006) 231–271
EARTH-SCIENCE REVIEWS
www.elsevier.com/locate/earscirev

Mantle plumes from top to bottom

Norman H. Sleep

Department of Geophysics, Stanford University, Stanford, California 94305, USA

Received 24 March 2005; accepted 20 March 2006
Available online 23 May 2006

Abstract

Hotspots include midplate features like Hawaii and on-axis features like Iceland. Mantle plumes are a well-posed hypothesis for their formation. Starting plume heads provide an explanation of brief episodes of flood basalts, mafic intrusions, and radial dike swarms. Yet the essence of the hypothesis hides deep in the mantle. Tests independent of surface geology and geochemistry to date have been at best tantalizing. It is productive to bare the current ignorance, rather than to dump the plume hypothesis. One finds potentially fruitful lines of inquiry using simple dynamics and observations. Ancient lithospheric xenoliths may reveal heating by plumes and subsequent thermal equilibration in the past. The effect at the base of the chemical layer is modest 50–100 K for transient heating by plume heads. Thinning of nonbuoyant platform lithosphere is readily observed but not directly attributable to plumes. The plume history in Antarctica is ill constrained because of poor geological exposure. This locality provides a worst case on what is known about surface evidence of hotspots. Direct detection of plume tail conduits in the mid-mantle is now at the edge of seismic resolution. Seismology does not provide adequate resolution of the deep mantle. We do not know the extent of a chemically dense dregs layer or whether superplume regions are cooler or hotter than an adiabat in equilibrium with the asthenosphere. Overall, mid-mantle seismology is most likely to give definitive results as plume conduits are the guts of the dynamic hypothesis. Finding them would bring unresolved deep and shallow processes into place.

Keywords: mantle plumes; hotspots; xenoliths; lithosphere; Antarctica; core–mantle boundary; tomography; geotherm

1. Introduction

Earth scientists apply the term “hotspot” to regions voluminous on-ridge volcanism, like Iceland, and sites of midplate volcanism, like Hawaii. The question arises as to whether both features have the same underlying cause, justifying the shared name. If so the mechanism needs to be recognized and understood. The mantle plume hypothesis of Morgan (1972) provides a viable and testable explanation for both features as well as flood basalts and radial dike swarms.

Plumes are clearly a simple concept for viewing part of the flow within the Earth, like a hurricane in meteorology. The concepts of mantle plumes and a typical (mid-ocean ridge basalt, MORB) mantle adiabat are linked. The excess temperature of the most of the material ascending in plumes is much greater than other ambient temperature variations in the asthenosphere. The plume concept is useful if that is in fact the case.

At first glance, plumes are geometrically simple. Cylindrical conduits of hot material ascend from great depths in the mantle (Fig. 1). They produce midplate hotspots when they impinge on the base of the lithosphere and on-ridge hotspots when they are close to ridge axes. In both cases, the plumes are sources of

E-mail address: norm@pangea.stanford.edu.

0012-8252/$ - see front matter © 2006 Elsevier B.V. All rights reserved.
doi:10.1016/j.earscirev.2006.03.007

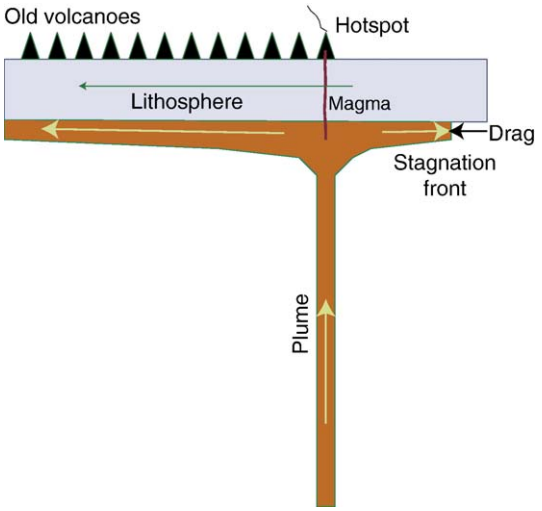

Fig. 1. Schematic diagram of a hotspot track produced by plume beneath fast-moving plate. A chain of volcanoes forms when the plate passes over the plume. Lateral flow of buoyant plume material complicates the flow pattern beneath the base of the lithosphere. The plate drags the plume material along with it. A stagnation front exists upstream of the hotspot.

hot material that flows buoyantly along the base of the lithosphere, not candle-like sources of heat (Fig. 2). Moreover, some midplate hotspots appear to have evolved into on-ridge hotspots and vice versa, indicating a common cause (Sleep, 1990a,b, 2002). The best example is Great Meteor track that includes the continental Monteregian Hills, the mid-oceanic New England Seamounts, the on-ridge Corner Seamounts, and the off-ridge Great Meteor Seamount on the African plate.

Plumes start with a massive head fed by a tail conduit. Short-lived voluminous volcanic events occur when plume heads arrive at the base of the lithosphere. Flood basalts and radial dike swarms provide evidence of the antiquity of this process.

Yet highly competent scientists question the existence of mantle plumes (e.g., Anderson, 2000; Foulger, 2002, Foulger et al., 2005). Some skepticism is warranted. The hypothesis is easily posed in a circular fashion. Hotspots indicate plumes, which shows that plumes cause hotspots. Such reasoning triggered my initial opposition to the hypothesis. This aside, the predictions of the plume hypothesis are plentiful, but they are also complicated, occur partly at great depth, and are not yet well understood.

The large literature on isotopic and trace-element geochemistry of mantle-derived rocks is beyond the scope of this paper. It is obvious that hot material should begin melting at greater depths and melt more than mantle at its usual temperature. I do not attempt to sort out these effects from the effects of ubiquitous chemical heterogeneities in the mantle on isotopes and trace elements (see Meibom et al., 2005).

Major element considerations give the plume material ascends ~200 K hotter than normal mantle (e.g., Putirka, 2005). (Ideally one should distinguish the typical excess temperature in the plume tail from the maximum excess at its center. Given the lack of hard constraints, I do not do this.) I use this temperature

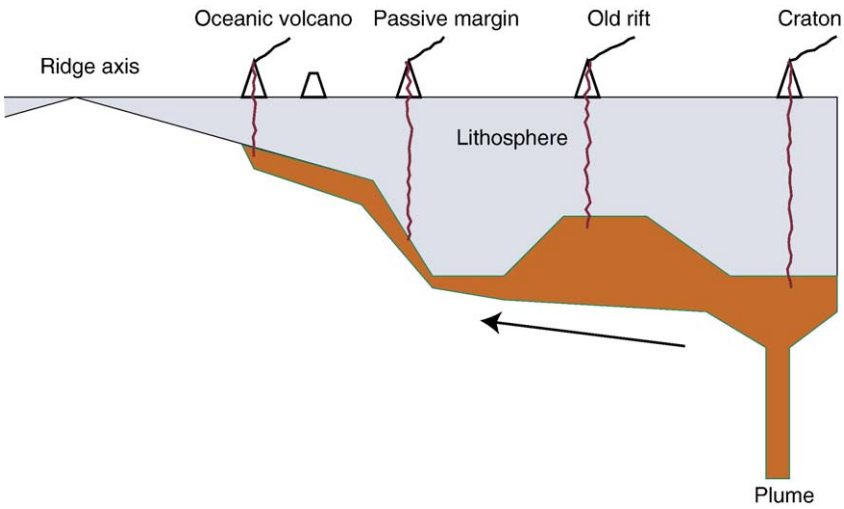

Fig. 2. Schematic diagram of the lateral flow of plume material beneath a slow-moving continent. The plume material ponds beneath locally thin lithosphere of an old rift. It "under bottoms" a region of thick lithosphere and cascades across a passive margin. It then flows toward the ridge axis, forming volcanoes along a flow line.

anomaly as a constraint to evaluate the dynamics of problems and 300 K when an upper bound is relevant.

I concentrate on other selected aspects of our ignorance where progress might be made. Plume proponents have yet to determine which hotspots directly overlie plumes, which are secondary hotspots from the lateral flow of plume material along the base of the lithosphere, and which merely result from cracks in the lithosphere allowing magma to ascend from sources within ordinary temperature mantle. Courtillot et al. (2003) discuss which hotspots are most likely to come from deep plumes. We lack adequate explanations for numerous volcanic features on land and beneath the sea. Cracks modulate hotspots; they are required for plume-sourced lavas to vent.

The lack of data from the ocean basins is a major problem. Over much of the Earth, we have only satellite gravity and bathymetry. This gives us the geometry and the usual oceanic hotspot tracks. We lack reliable ages and reliable paleomagnetics to give the latitude of formation.

Finally, plumes are really a group of partly disjoint hypotheses. Recognition that hot material has arrived at the base of the lithosphere does not directly constrain how this material originated (became hot) at great depth and how it then ascended to lithospheric depths. For example, Wilson (1963) placed the source of material for his hotspot within the core of a convection cell.

In this review, I consider some aspects of the detection of mantle plumes in the past and the present. To avoid cluttering the paper with weaseling qualifiers, I continue to presume that plumes exist so that I can make inferences that lead to new testable predictions. I concentrate on topics that may provide such additional constraints, rather than reviewing the well established evidence of hotspot features. I begin with the base of the lithosphere to introduce the physical processes that affect plume material once it has ascended. I then present Antarctica as a remote and hence poorly understood example of the complexity of lateral flow of plume material beneath the lithosphere. It provides a possible example involving the interaction of starting plume heads at mid-mantle depths. I work downward in the Earth discussing plume conduits at mid-mantle depths and finally the source of plumes in the deep mantle.

My intent is to make the plume hypothesis more testable while pointing out areas of ignorance. Like with stellar parallax in the time of Galileo and Newton, it is valuable to constrain the size of effects before we try to detect them and especially before we claim they do not exist. We should not jettison a well-posed hypothesis just because its complicated effects are not yet resolved.

Alternatives to plumes involve cracks that let magmas vent from widespread source regions of the mantle. Crack hypotheses for major hotspots have not become much more focused since Wilson (1963) reviewed them. I spent considerable time attempting to find a viable one early in my career. I thus concentrate on discussing potential positive evidence for plumes. I review mechanism where shear–strain heating at the base of moving plates generates hotspots in Appendix A.

2. Ponded plume material and the thermal history of the base of the lithosphere

In the "standard" form of the mantle plume hypothesis, hot material ascends buoyantly from great depths until it impinges on the cool base of the very viscous lithosphere (Fig. 1). The plume mantle then spreads laterally exchanging heat with the lithosphere by conduction and convection (Fig. 2). After a period of time, the plume material cools to the mantle adiabat, leaving the base of the lithosphere (defined by some isotherm) shallower and the material in the deep lithosphere hotter than it was before the plume impinged. Thereafter, the deep lithosphere cools and its base gradually returns to its former depth. The surface features associated with this process include volcanism when the plume material is present and uplift at the time the plume material impinges followed by subsidence as the lithosphere cools.

One would like to find direct evidence from the subsurface of past plumes to compare with surface geological history. The deep lithosphere of cratonal regions may keep this record. The basement of these regions is predominately Archean, over 2.5 Ga. (Ga is billion years before present, B.Y. is interval of 1 billion years.) Since then the cratons have been stable, but not altogether quiescent.

Modern geochronology indicates that stability extends to great depths in the lithosphere. Xenoliths from diamond pipes and other igneous rocks sample that the lithosphere down to ~200-km depth (Boyd et al., 1985; Carlson et al., 1999; Griffin et al., 1999; Pearson, 1999; Saltzer et al., 2001; Schmidberger et al., 2002; Irvine et al., 2003; Griffin et al., 2003a; Shirey et al., 2003, 2004; Carlson and Moore, 2004; Lehtonen et al., 2004). Subsequent to its stabilization, the cratonal lithosphere has experienced discrete events, as did the surface. These include activity attributed to plumes, subduction, continental collision, and continental break-up (Griffin et al., 2003a,b; Shirey et al., 2003, 2004; Bleeker, 2003; Schulze et al., 2004).

Mineralogical studies of the xenoliths constrain the temperature and pressure of their environment just before the time of their ascent, giving an instantaneous geotherm (temperature as a function of depth) (e.g., Rudnick and Nyblade, 1999; Bell et al., 2003). Radiometric dating of eruption time is effective (e.g., Heaman et al., 2004). Multiple ages of kimberlites exist in some areas, especially southern Africa. This gives information on the history of the geotherm over geological time (Bell et al., 2003). This is a potential way to detect heating associated with plume material ponded at the base of the lithosphere (Sleep, 2003a).

The Minas Gerais region of Brazil provides a well-timed example of lithospheric thinning that may have a relationship to plumes (Read et al., 2004). This area, west of the Archean São Francisco craton, has Proterozoic basement that may have been underlain by ordinary (not chemically buoyant) mantle. Between 95 to 85 Ma, diamond-bearing kimberlites erupted in this region through lithosphere with a cratonal geothermal gradient. (Ma is million years before present; m.y. is an interval of 1 million years.) Immediately thereafter between ~84 and 61 Ma, diamond-free kamafugites erupted through much thinner lithosphere. The temperature at ~150 km depth increased by ~240 K between the two igneous episodes.

The quick lithospheric thinning leads me to invoke impingement of plume material at the base of the lithosphere as a hypothesis (Fig. 3). This region and its younger volcanism lie along an ill-defined slowly moving plume track (Sleep, 2003c). The present plume as imaged by tomography is southeast of Minas Gerais (Schimmel et al., 2003). The hypothesized plume was to the northwest under the Guaporé shield at the kamafugite eruption time. In this plume hypothesis, buoyant plume material flowed from beneath thick lithosphere at the plume orifice beneath the Guaporé shield to locally thinner lithosphere beneath Minas

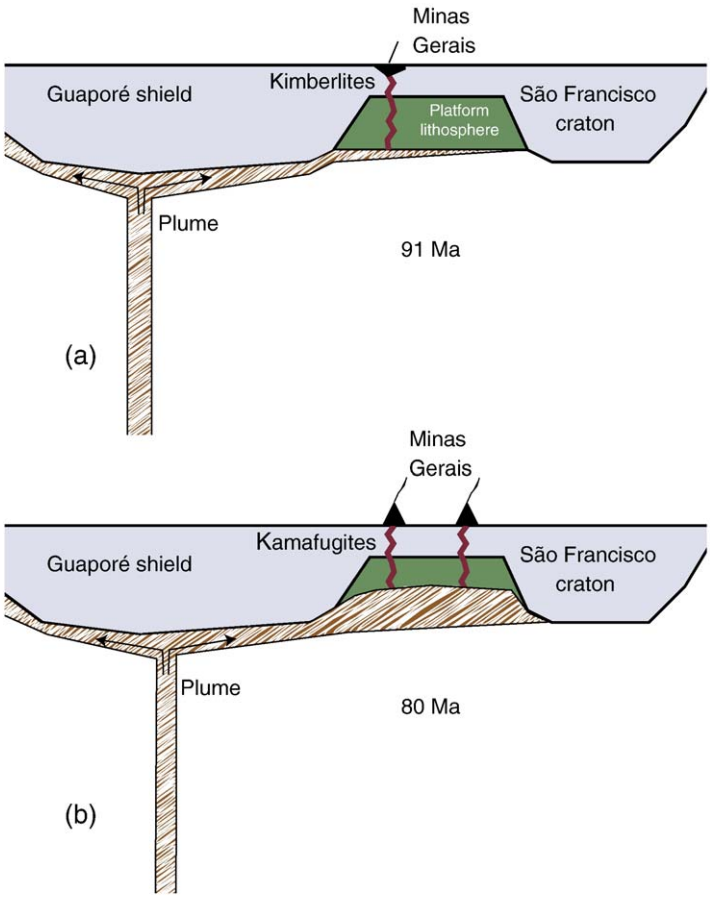

Fig. 3. Schematic diagram of the history of platform lithosphere beneath Minas Garais, Brazil. (a) At 91 Ma, the plume is to the northwest beneath the Guaporé shield. Plume material begins spilling beneath Mainas Gerais producing diamond-bearing kimberlites. (b) By 81 Ma, plume material has ponded beneath Minas Gerais. Kamafugites erupt through thinned platform lithosphere.

Gerais where it ponded. (Feng et al. (2004) resolve thick lithosphere beneath the Guaporé shield and the São Francisco craton with surface wave tomography.) It then convectively thinned the non-chemically buoyant Minas Gerais lithosphere quickly increasing the temperature at ~150 km depth.

More powerful methods of detecting temperature changes over time are conceivable. Growth rings in diamond crystals indicate the passage of time during growth (Schulze et al., 2003a,b, 2004). These rings provide relative dates for mineral inclusions within the diamond. Phillips et al. (2004) distinguish touching inclusions that record conditions just before the time of kimberlite eruption from nontouching inclusions that record conditions at the time of crystallization of that part of the diamond. In their case, the diamond was hotter at ~3 Ga than at ~85 Ma when it erupted. Studies of the radiogenic isotopes and mineralogy within a suite the inclusions could provide pressure–temperature–time paths. For example, Davis et al. (2004) distinguish diamonds formed at great depth within an ascending plume from resident diamonds at the base of the lithosphere.

Although these methods might not give detailed histories for resident diamonds in practice, I compute theoretical depth–temperature–time paths to constrain the expected effects of plumes. I begin with theoretical constraints on such paths with southern Africa and plumes in mind. O'Neill and Moresi (2003) discuss temperature changes associated with subduction and plate movements.

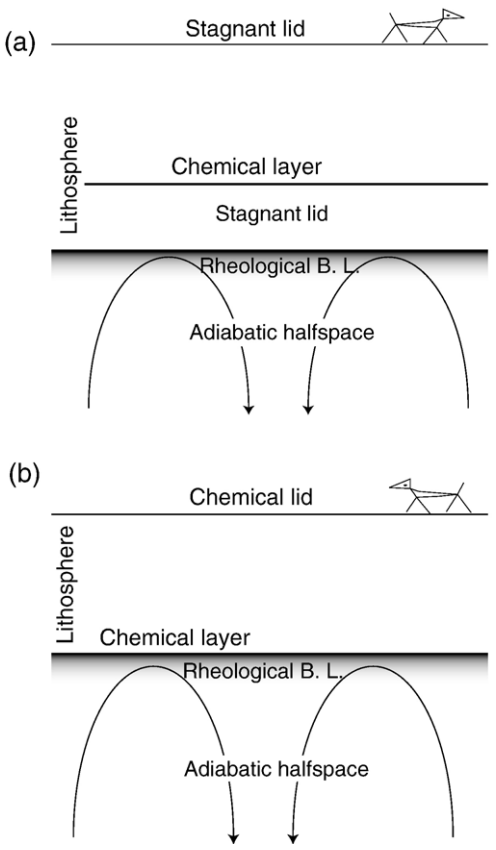

Fig. 4. Schematic diagram shows the difference between stagnant-lid convection (a) and chemical-lid lid convection (b). Only the temperature contrast within the rheological boundary layer drives flow.

2.1. Convection beneath a chemical lid

I begin with the usual state of the lithosphere to put the aftermath of plumes in context. Cratonal lithosphere is chemically buoyant relative to normal mantle (Fig. 4). Seismic data provide regional averages while xenoliths provide point samples (Griffin et al., 2003a; Shirey et al., 2003, 2004). In general, the two data sets agree enough to delineate volumes of fertile and depleted lithosphere (e.g., Kopylova et al., 2004; Shirey et al., 2004). Geoid and isostasy studies confirm the buoyancy but have poor depth resolution (Shapiro et al., 1999a, b; Mooney and Vidale, 2003). It particular, it is not clear whether (and where) the buoyant lithosphere currently provides a lid above convection in the underlying mantle.

In terms of fluid dynamics, a rheological boundary layer exists between the lithosphere and the underlying adiabatic mantle (Fig. 4). The rheological boundary layer feeds downwellings of cool material into the mantle. The underlying mantle upwells, maintaining mass balance. Cool ordinary mantle material may cap the convection. It does so by being very viscous. Fluid dynamicists refer to this situation as stagnant-lid convection (e.g., Solomatov, 1995; Solomatov and Moresi, 2000). Alternatively, the chemical layer caps the flow (Lenardic and Moresi, 2003). It resists downwelling by being buoyant and more viscous than ordinary lithosphere (Lenardic et al., 2003; Sleep, 2003b). I refer to this situation as chemical-lid convection in analogy to stagnant-lid convection.

On the present Earth, cratonal lithosphere with a chemical lid is only modestly thicker than platform lithosphere where a chemical lid is unlikely (e.g., Kaminski and Jaupart, 2000). This implies the chemically buoyant layer beneath cratons does not greatly affect lithospheric thickness or convection. In fluid dynamic terms, the chemical-lid convection beneath cratons is transitional to stagnant-lid convection. I can thus use the well-known stagnant-lid scaling relationships (Davaille and Jaupart, 1993a,b, 1994; Solomatov,

1995; Solomatov and Moresi, 2000) to make general inferences about cratonal thermal structure.

Two predictable and observable aspects of convection beneath the lithosphere are the laterally averaged heat flow and the temperature contrast across the rheological boundary layer. I restrict discussion to a linear (Newtonian) viscosity. To obtain simple revealing relationships and numerical models, I assume a simple temperature- and chemical-dependent rheology where the viscosity is given by

$$\eta = \eta_0 \exp\left[\frac{\Delta T}{T_\eta}\right]\left[\frac{\eta_C}{\eta_0}\right]^{\phi}, \tag{1}$$

where η_0 is the viscosity of ordinary mantle at the reference temperature of the mantle adiabat, η_C is the viscosity of chemically different continental lithosphere at the reference temperature, ϕ is the fraction of continental lithosphere within a (numerical) domain, ΔT is the temperature below the mantle adiabat, and T_η is the temperature scale for viscosity (Doin et al., 1997; Sleep, 2003b). The laterally averaged heat flow through a stagnant lid at steady state is

$$q_{SS} \approx 0.47 k T_\eta \left[\frac{\rho g \alpha T_\eta^3}{\kappa \eta}\right]^{1/3} \tag{2}$$

where k is thermal conductivity, ρ is density, g is the acceleration of gravity, α is the volume thermal expansion coefficient, η is the viscosity of the underlying half-space, and $\kappa \equiv \rho C$, where C is specific heat per mass. The leading coefficient 0.47 comes from laboratory and numerical experiments. The temperature contrast across the rheological boundary layer is

$$\Delta T_{rheo} = \beta T_\eta \tag{3}$$

where β is a dimensionless constant of the order of a few. The value of β is somewhat arbitrary as viscosity, velocity, convective and conductive heat flow, and stress vary continuously. The usually quoted value comes from the depth where laterally averaged convective heat flow is evident in a physical or numerical experiment. Davaille and Jaupart (1993a,b, 1994) and Solomatov and Moresi (2000) give 2.3 and 2.4, respectively. For my purposes, a more stringent criterion is relevant (Fig. 4), defined by temperature where replacing the isochemical stagnant lid with a chemical lid or a rigid region as no effect on the laterally averaged heat flow. As shown below, β defined in this way is over 3.5. To make this distinction, I let the temperature contrast beneath the chemical lid be ΔT_{lid}. The maximum value of ΔT_{lid} that affects convection is ΔT_{rheo} in Eq. (3).

2.2. Buoyancy and uplift

Uplift and later subsidence is a geologically observable consequence of plume material ponding at the base of the lithosphere. I ignore chemical buoyancy for simplicity because I am interested in transient temperature changes beneath stable lithosphere. The uplift beneath air is

$$\Delta E = -\int \alpha \Delta T dz, \tag{4}$$

where z is depth and the minus sign occurs since I define ΔT as a temperature decrease. The change in the heat within a column of unit area is given by a homologous integral

$$\Delta Q = -\int \rho C \Delta T dz, \tag{5}$$

If no heat is added or lost from the bottom, the surface heat flow is

$$q = \frac{\partial \Delta Q}{\partial t} \tag{6}$$

where t is time. Combining Eqs. (4)–(6) gives the O'Connell relationship for the subsidence rate,

$$-\frac{\partial \Delta E}{\partial t} = q\left[\frac{\alpha}{\rho C}\right] \tag{7}$$

In general, the subsidence rate is proportional to the net heat flow out of the top and into the base of the lithosphere, accounting for heat flow associated with radioactive decay mainly in the crust. The terms in the bracket in Eq. (7) are reasonably well constrained, $\alpha = 3 \times 10^{-5}$ K^{-1} and $\rho C = 4 \times 10^6$ J m^{-3} K^{-1}. In more geological units, 1 W m^{-2} of heat flow gives 236 m per million years of subsidence.

I assume a linear steady-state temperature gradient in the stagnant lid and the chemical lid to get simple expressions for elevation changes. That is, I assume thermal conductivity is constant, ignore the continental crust and its radioactive heat sources. The simplest model is a linear temperature gradient to the mantle adiabat. That is,

$$\Delta T = T_L(1 - z/Z_L) \tag{8}$$

where T_L is the temperature at the base of the lithosphere (the surface is 0 °C) and Z_L is the lithosphere thickness. The elevation change relative to adiabatic mantle is simply $\alpha T_L Z_L / 2$. A more sophisticated approximation includes the temperature variation

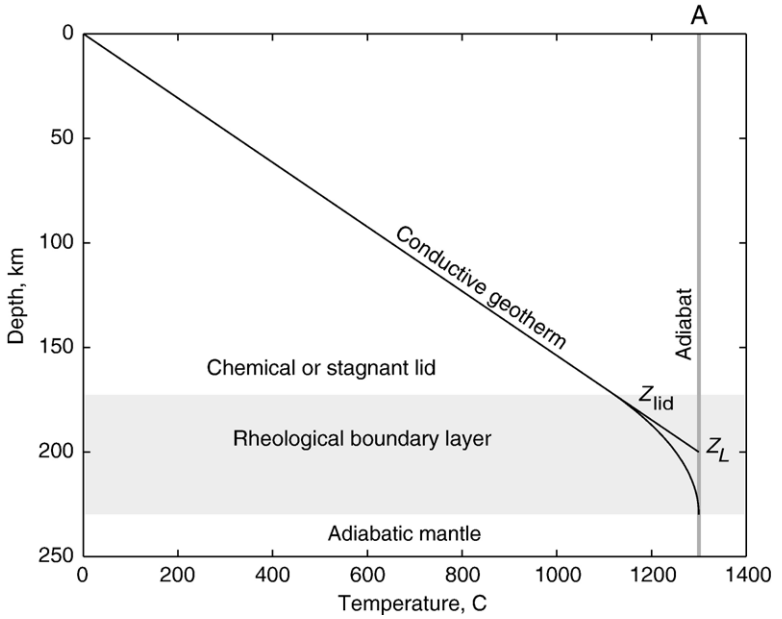

Fig. 5. Potential temperature within the lithosphere in °C. The laterally averaged geotherm changes from the linear conductive gradient to the adiabat within the rheological boundary layer. The crust is ignored.

within the boundary layer beneath either a chemical or stagnant lid (Fig. 5). Eq. (8) then applies within the lid shallower than $z=Z_{lid}$ where the temperature deficit is $\Delta T_{lid}=T_L(1-Z_{lid}/Z_L)$, where Z_L is now the more general scale thickness of the lithosphere from extrapolating the conductive geotherm to the mantle adiabat. The heat flow and thermal gradient decrease linearly to zero at the depth $Z_B=2Z_LZ_{lid}$

$$\Delta T = \frac{T_L(2Z_L-Z_{lid}-z)^2}{4Z_L(Z_L-Z_{lid})}. \quad (9)$$

The depth-integrated temperature deficit in the boundary layer is

$$\frac{2T_L(Z_L-Z_{lid})^2}{3Z_L}. \quad (10)$$

The integrated temperature anomaly in the lid plus the boundary layer is

$$\frac{T_LZ_L}{2}+\frac{T_L(Z_L-Z_{lid})^2}{6Z_L} \quad (11)$$

where the first term is the temperature anomaly obtained by linearly extrapolating the geotherm in the lid and the second term is the small effect of the boundary layer. The second term is small enough that I ignore it in quick calculations.

2.3. Numerical models

I present numerical models to illustrate the temperature changes that occur near of the base of the lithosphere. The numerical method and material parameters are the same as used by Nyblade and Sleep (2003). Certain parameters are well enough constrained and vary little enough in the uppermost mantle that they can be considered constants. These include the thermal expansion coefficient $\alpha=3\times10^{-5}$ K^{-1}, volume specific heat $\rho C=4\times10^6$ J m^{-3} K^{-1}, thermal conductivity $k=3$ W m^{-1} K^{-1}, the potential temperature of the mantle adiabat $T_L=1300$ °C, the density $\rho=3400$ kg m^{-3}, and the acceleration of gravity 9.8 m s^{-2}.

Rheological parameters are less well constrained. I let T_η be 60 K in all the models and let the scaling in Eqs. (2) and (3) generalize my results. I use two values of viscosity η_0, 0.4×10^{19} and 0.653×10^{19} Pa s. They have expected stagnant-lid heat flows of 23.0 and 19.5 mW m^{-2} and scale thickness of the lithosphere Z_L of 170 and 200 km, respectively.

I do not vary the parameters representing the chemical lithosphere because they are somewhat constrained by mineral physics and previous modeling (Doin et al., 1997; Sleep, 2003b). In the calculations, the chemical lithosphere is a factor of 20 times more viscous and 50 kg m^{-3} less dense than normal mantle. I make the initial base of the chemical lithosphere 177.5 km by setting φ to 1 in all grid nodes from 175 km to the

surface and to zero below that. The depth is motivated by the results of Saltzer et al. (2001) for southern Africa and Lehtonen et al. (2004) for Finland. The reader can rescale to another depth as nearby effects of the interface depend on the distance from it.

The domain of the model is 1500 km horizontal by 500 km vertical. I apply the natural boundary condition of free slip and constant temperature 0 °C at the surface. I apply symmetry conditions of no lateral flow, no lateral heat flow, and free slip at the side boundary and concentrate on the middle of the model away from the boundaries. I apply a permeable boundary condition to the base where material enters at the mantle adiabat. The velocity is perpendicular to this boundary. Mathematically the boundary does no work on the domain of the calculation. I start the models with a linear temperature gradient that intersects the mantle adiabat at 200-km depth. Below that the temperature is at the mantle adiabat except for a small random perturbation at all points at 210-km depth to trigger convection. The calculations are deterministic, but the vagaries of convection depend on the perturbation.

2.4. Numerical results

Numerical models without plumes put their effects in context (Figs. 6–8). Model 1 differs from model 2 by having a somewhat higher high flow (17.9 mW m^{-2} versus 15.7 mW m^{-2}), which is expected since it has lower viscosity along the mantle adiabat. Using the heat flows, the steady state temperature at the base of the chemical layer at 177.5 km depth is 1059 and 929 °C, respectively. These temperature contrasts with the mantle adiabat ΔT_{lid} divided by T_{η} are 4.0 and 6.2, respectively. The models are not quite to steady state. The actual normalized temperature contrasts are 3.6 and 4.2, respectively. Having the laterally averaged heat flow slightly below steady state may sometimes be realistic, as lithosphere is likely to be cooling from previous plume events and from the general decrease in the Earth's interior temperature over geological time.

Passive marker particles monitor the temperature history of material started just within the chemical layer (175-km depth) and just below the chemical layer (180-km depth) over the last 50 m.y. of the calculation (Fig. 7). The gradual long-term cooling of the model is not evident from fluctuations in model 1. Fluctuations about the mean are 10–20 °C at 180 km and ~15 °C at 175 km. They are ~12 and ~10 °C, respectively about the long-term trend in model 2. Such ambient fluctuations constitute noise if one wishes to look for the effects of plumes. The temperature fluctuations of marker particles (as would be observed from diamond inclusions) are less than the fluctuations at a fixed depth. Material tends to move upward towards cold when it is in hot upwellings and downward when it is within cool downwellings. The effect is significant as moving 1 km

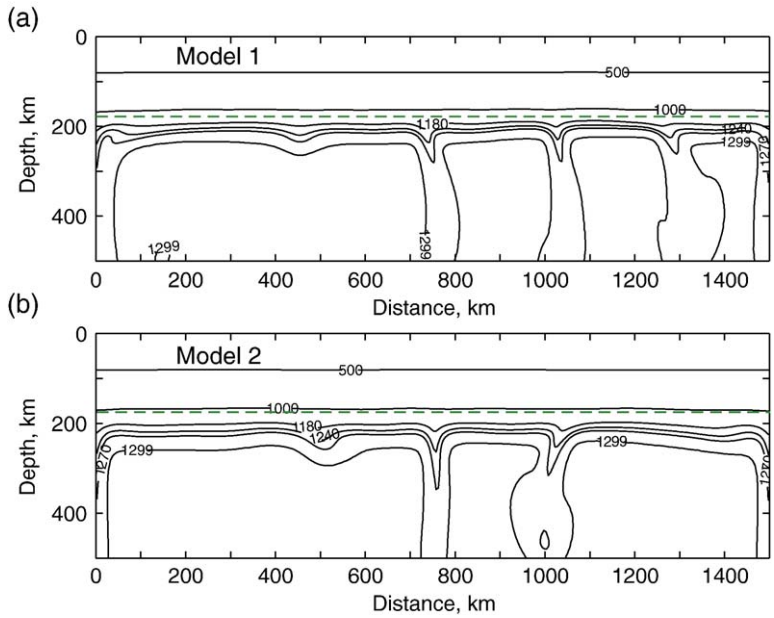

Fig. 6. Potential temperature isotherms in °C for model 1 (a) and model 2 (b) 150 m.y. after the start of convection. The dashed line is the base of the chemical lid. This is the starting condition before the plume material was introduced. The horizontal distance is 0 at the left-side artificial boundary.

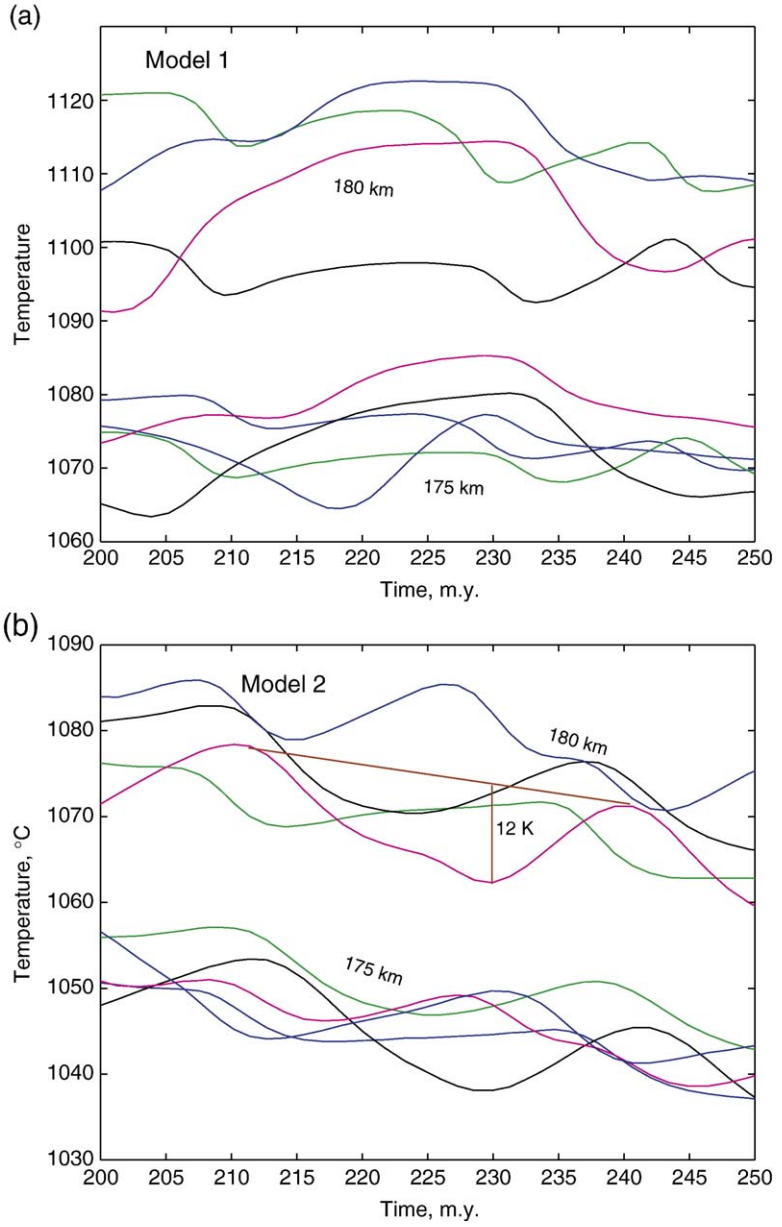

Fig. 7. Potential temperature–time paths for marker particles started at 175 and 180 km depth. (a) The temperature in model 1 has approached quasisteady state. No trend is evident in the oscillations. (b) Model 2 is still cooling. The deviations from the trend at 180 km are about 12 K. This diagram illustrates the ambient effects of unsteady convection in the absence of plumes.

in the average conductive thermal gradient changes temperature by ~6 K.

Fig. 7 shows material paths. The vertical movement is ~1 km for particles started at 175-km depth and a few kilometers for particles started at 180-km depth. Particles started at 185-km depth move around a lot and sometimes get swept into downwellings. One would not expect material at this depth to remain with the lithosphere since the Archean.

I start a plume at 249.9 m.y., just before the results discussed above. I cannot represent a cylindrical plume conduit in two-dimensions. Following Nyblade and Sleep (2003), I introduce a batch of plume material in a rectangular region between 350 and 450-km depth and 550 to 950-km horizontal distance. It has excess temperature of 300 K. The material entrains normal mantle on the way up and spreads out laterally over the base of the model. It is equivalent to a 40-km thick layer

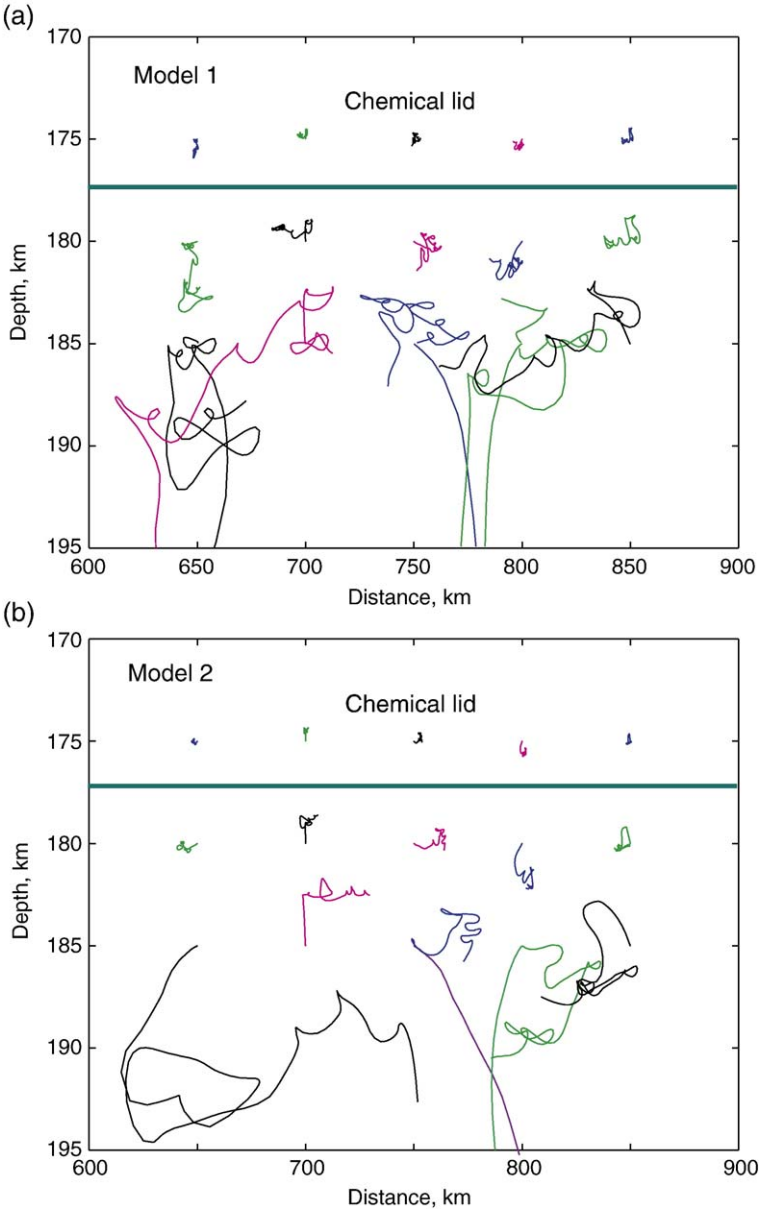

Fig. 8. Depth–distance plots of the marker particles in Fig. 8 with additional particles started at 185 km depth for model 1 (a) and model 2 (b). The program reseeds particles that go off the base of grid. Vertical exaggeration is 10 to 1.

with an excess temperature of 200 K across the 1500-km base of the model. That is, the excess temperature in a column of unit area is 8000 K km. I intend the models to represent the aftermath of the arrival of a starting plume head or the brief impingement of a plume tail.

The ponded plume material convects vigorously at its top and is stably stratified at its bottom (Fig. 9). The mantle plume does not contain enough heat to remove the rheological boundary layer, which has a temperature deficit in a column of unit area of 5300 K km, as some heat conducts upward into the boundary layer. Quantitatively, the heat per area supplied by the plume is equivalent to 37 m.y. of preplume heat flow through the lid.

The typical temperature increase following the plume at 175 and 180-km depth is 50 and 70 K, respectively (Fig. 9). Temperature reaches a maximum ~25 m.y. after the plume and approaches its preplume value ~100 m.y. after the plume. Material originally at 175-km depth moves vertically by over a kilometer. Material originally

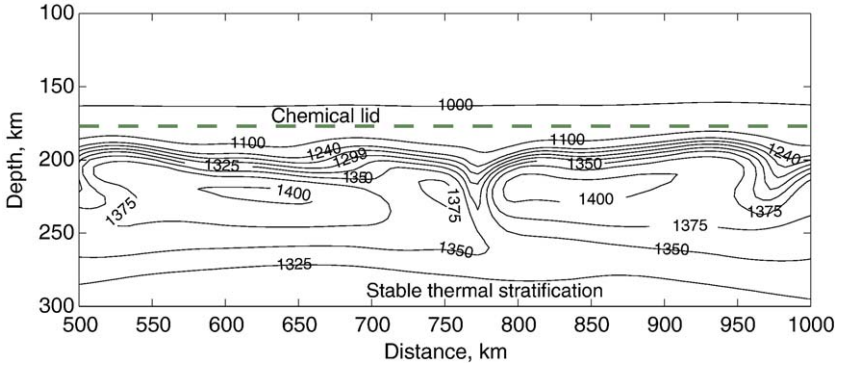

Fig. 9. Plume material ponds beneath the lithosphere in model 1, 5 m.y. after plume material was introduced. The plume material convects. The stable chemical stratification at the top (dashed line) and the stable thermal stratification at the bottom limit the domain of active convection.

at 180-km depth moves a few kilometers, but one of the tracers moved down to 193-km depth where it will eventually downwell. Several particles started at 185-km depth downwelled out of the window of the model.

A second calculation represents the effects of a plume that lingers beneath the lithosphere. I impose a second batch of plume material identical to the first at 263 m.y. The temperature increases ~100 K at 175-km depth and ~140 K at 180-km depth (Fig. 10). That is, the temperature increase scales linearly with the heat per area supplied by the plume. This allows interpolation and extrapolation with the caveat that the plume cannot heat the base of the lithosphere above its own temperature. Temperature peaks about 35 m.y. after the first plume. The particles move more than in the calculation with 1 plume event (Fig. 11).

The effects do not depend strongly on the preplume temperature at the base of the chemical lid, which is significantly cooler in model 2 than model 1 (Fig. 12). The wanderings of markers and the temperature changes of ~50 K at 175-km depth and ~70 K at 180-km depth are similar to model 1. The temperature peaks later than in model 1, about 35 m.y. after the plume event.

The retention of lithospheric material over time is relevant to the existence of ancient deep xenoliths. All the plotted particles shown within the chemical layer stayed near their starting positions. Some of the material originally 2.5 km beneath the interface got entrained into deeper flow, particularly after plumes impinged. Particles started 7.5 km below the interface tended to stray from the lithosphere. Weak relief ~2 km developed on the chemical interface (Fig. 13).

Some of the chemical layer got entrained to depth particularly at the ends of the model where downwellings persist (Fig. 6). The entrainment of only ~1 km of the chemical layer over 350 m.y. is acceptable with regard to the persistence of deep Archean lithosphere as sampled by xenoliths. The amount is not well resolved by the model as it is much less than the 5-km numerical grid spacing. This is a general failing of currently feasible numerical calculations that does not affect the rest of the output (e.g., McNamara and Zhong, 2004). Mathematically, the model represents composition with a linear gradient between grids. This interpolation leads to averaging and hence numerical dispersion. In my code, numerical dispersion is zero when velocity is in the cardinal directions and greatest on the flanks of downwellings where the velocity is inclined 45° to the grid. In general, dispersion increases the calculated amount of entrainment so the amount in Fig. 13 is an upper limit. Physically, a type of dispersion occurs in the flowing mantle. Viewed in detail, the base of the chemical lithosphere, like the rest of the Earth, is a mixture of various rock types that when spatially averaged is a gradient, not a clean interface. One should include such heterogeneity in high-resolution numerical models.

2.5. Nearly fixed plume

I now consider the limit of a plume that lingers beneath chemical lithosphere for a long period of time so that the geotherm comes into equilibrium. For an example of the geotherm before a prolonged plume event, I let the scale thickness of the preplume lithosphere be 210 km and the underlying adiabat be 1300 °C. To represent heating in the conductive lid, I fix the temperature at 180-km depth to 1500 °C beneath the assumed preplume geotherm. For an example of the aftermath of a prolonged plume event, I let the temperature be a linear gradient to the plume tem-

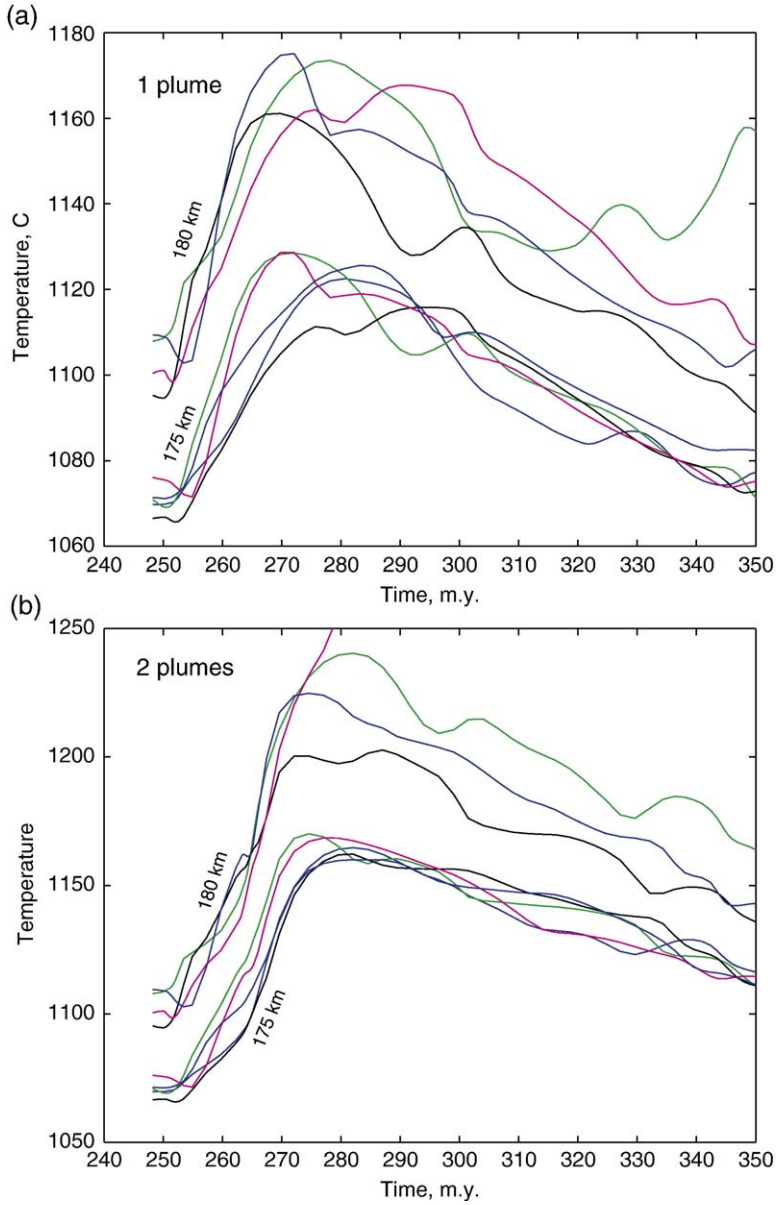

Fig. 10. Potential temperature–time plots for particles started at 175 and 180 km depth in the aftermath of 1 plume (a) and 2 plumes (b) for model 1. Gradual cooling follows quick heating except for particles entrained to greater depths.

perature of 1500 °C at the base of the chemical lid at 180-km depth. It is for simplicity the mantle adiabat 1300 °C below that (Fig. 14). I let this model cool by conduction.

As noted by Nyblade and Sleep (2003), plume material is ineffective at producing lofty mountains. The difference in elevation before and after the example plume event is 1125 m. For comparison, a 100-km column of plume material with an excess temperature of 200 K produces an uplift of 600 m. Plumes are potentially more effective uplift mechanisms beneath platforms underlain by ordinary mantle as hypothesized for Minas Gerais, Brazil on the basis of xenolith geotherms obtained by Read et al. (2004). For example, an event that changed the scale thickness to the mantle adiabat from 210 to 140 km would produce 1365 m of uplift.

The time dependence of plume effects is relevant. Surface heat flow, the geotherm near the base of the lithosphere, and elevation changes are observable.

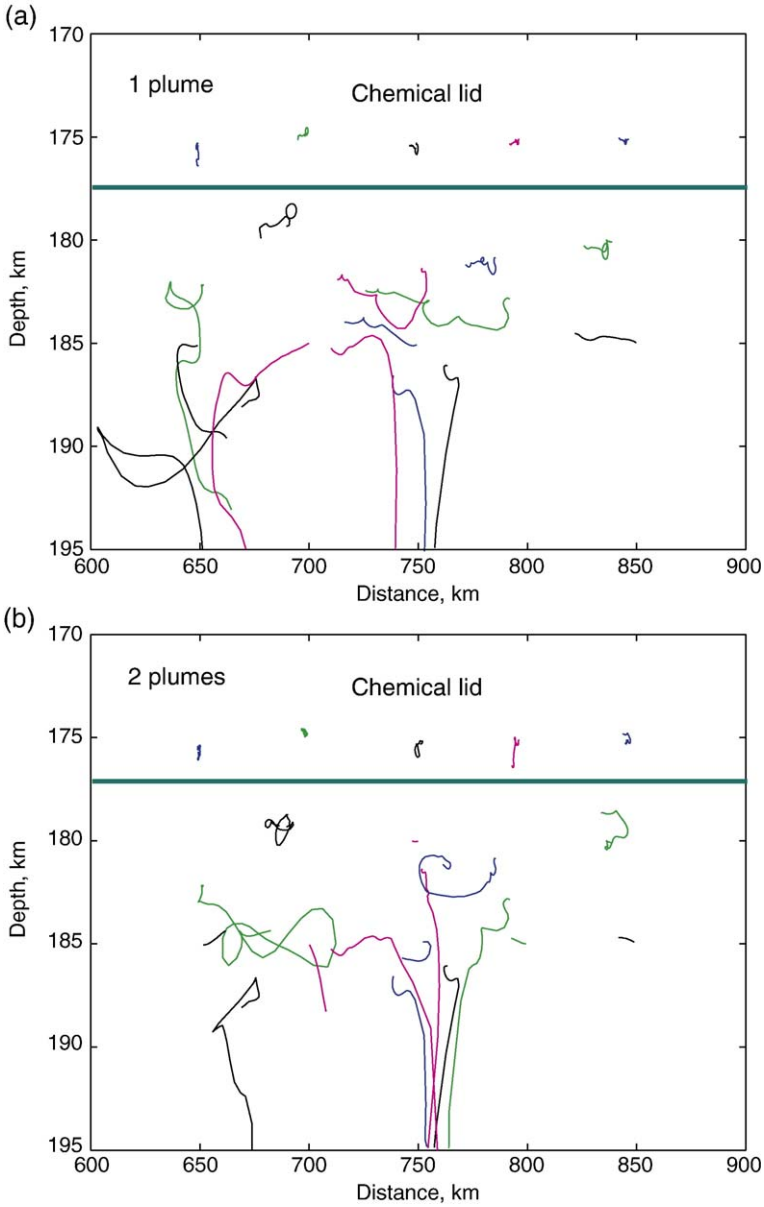

Fig. 11. Particle paths, as in Fig. 8, show the aftermath of 1 plume (a) and 2 plumes (b) for model 1. Note that several particles started at 180 km depth leave the base of the lithosphere.

These quantities change on a time scale proportional to the square of the distance from the base of the lithosphere. The land surface is far way from the plume material and heat flow changes slowly. The deep geotherm changes fast. Elevation involves the intermediate case of temperature in the middle of the lithosphere.

Plumes beneath chemical lids modestly change the surface heat flow even if steady state is reached (Nyblade and Sleep, 2003). In the example, the heat flow changes only from 18.6 to 25 mW m^{-2} between the preplume and final states. As a practical matter, surface heat flow is a long term average of the conditions at the base of the lithosphere. It takes hundreds of million years for the heat flow at the surface to respond to the conditions at depth (Figs. 15 and 16). Surface heat flow measurements alone are not useful in seeing this difference as regional variations in crustal radioactivity have larger effects. Xenolith data from kimberlites (Bell et al., 2003) or

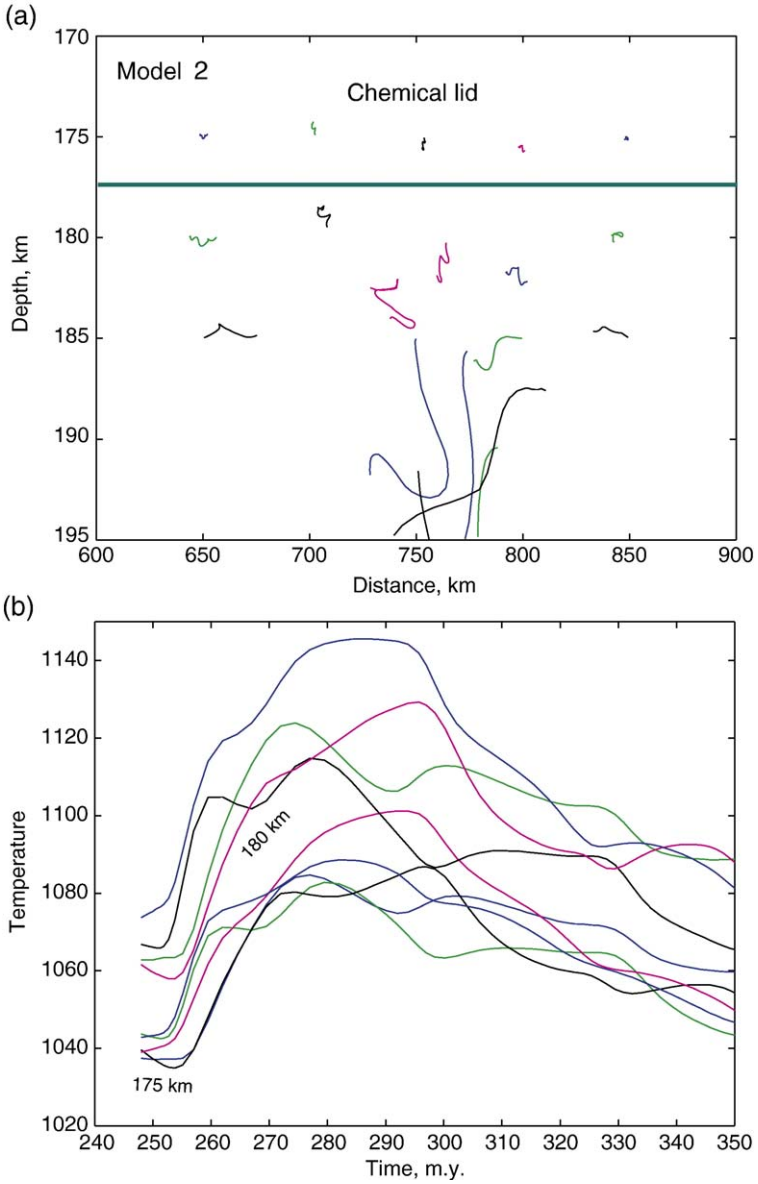

Fig. 12. Particle paths (a) and potential temperature–time paths (b) for model 2 show the aftermath of 1 plume.

potentially inclusions in diamonds resolve the geotherm deep in the lithosphere where it actually changes during and immediately following a plume event (Figs. 15 and 16).

Subsidence is observable in sedimentary basins (e.g., Kaminski and Jaupart, 2000). The physics of the aftermath of a plume are straightforward. Initially, the geotherm is stably stratified at the base of the lithosphere (Fig. 14). There is no convective heat flow at the base of the lithosphere. The previous heat flow continues at the surface. The initial subsidence rate beneath air from Eq. (7) is ~ 6 m m.y.$^{-1}$. The temperature anomaly ΔT_{lid} beneath the chemical layer drives convection. The base of the lithosphere cools to the mantle adiabat by 20 m.y. (Fig. 15). Until then, convection does not occur. For some time after that, convection is sluggish and the conductive calculation is a good approximation. Mathematically, convective heat flow scales with the temperature difference as $\Delta T_{\mathrm{lid}}/T_{\eta}$ to the $\sim 4/3$ power. It takes well over 100 m.y. for this ratio to approach its preplume value >3. Once this happens, convective heat flow is a significant fraction of surface heat flow and the conductive model no longer gives the laterally averaged temperature.

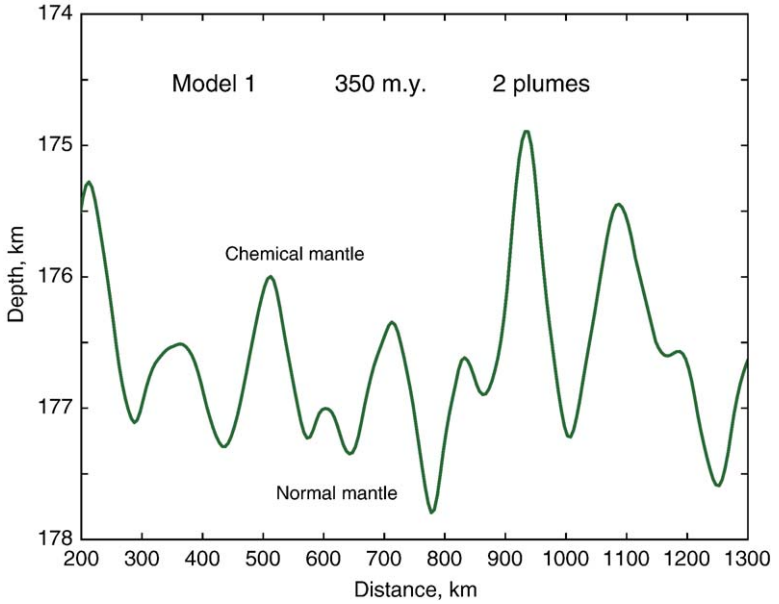

Fig. 13. Relief on the base of the chemical lithosphere for model 1 with 2 plumes 100 m.y. after the first plume started. The numerical parameter representing chemical composition $\phi = 1/2$ defines the line.

However, it does provide an upper limit on subsidence rate and an upper limit on ΔT_{lid}.

2.6. Overview of the base of the lithosphere

Xenoliths and diamond inclusions at the base of the lithosphere provide a record of temperature changes at the base of the lithosphere. The changes are expected to be subtle within chemically stable lithosphere, <100 K, unless the plume lingers for 10s of million years or thick plume material ponds within a region of locally thin lithosphere. The uplifts and subsequence subsidence is also expected to be <100s of meters with the same exceptions. Convective thinning of ordinary mantle

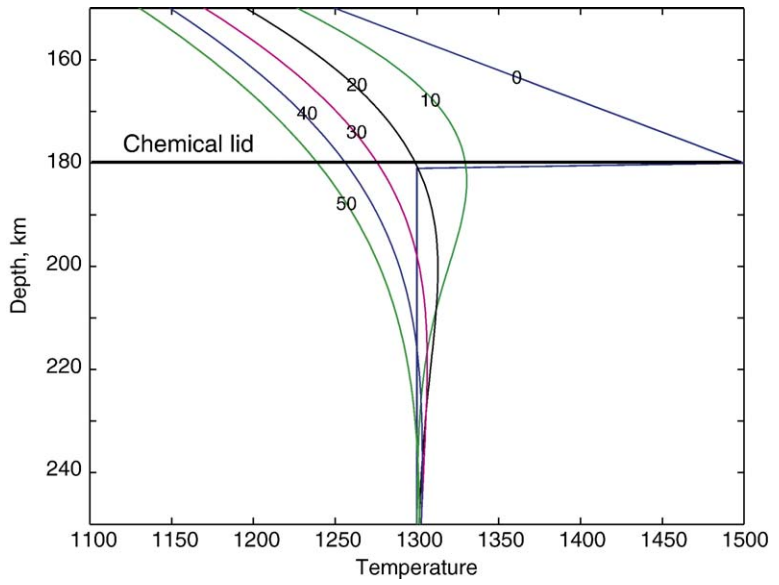

Fig. 14. Geotherms (labeled in m.y. from start of model) in a conductive model started with the mantle adiabat below 180 km depth and a conductive geotherm in equilibrium with plume material at 1500 °C above that. Only the temperature anomaly beneath the chemical lid can drive convection.

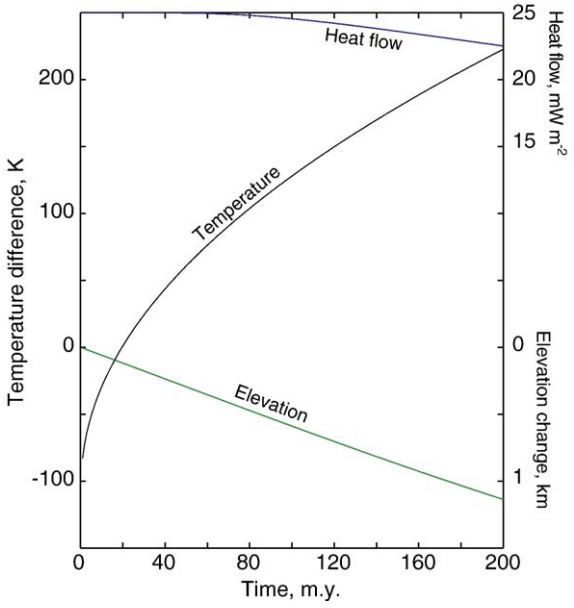

Fig. 15. The temperature difference between the base of the chemical layer and the mantle adiabat for the model in Fig. 14. The model becomes invalid once this difference is large enough to drive vigorous convection. The elevation changes steadily as heat escapes from the surface while no heat by assumption is added from below. The surface heat flow changes slowly.

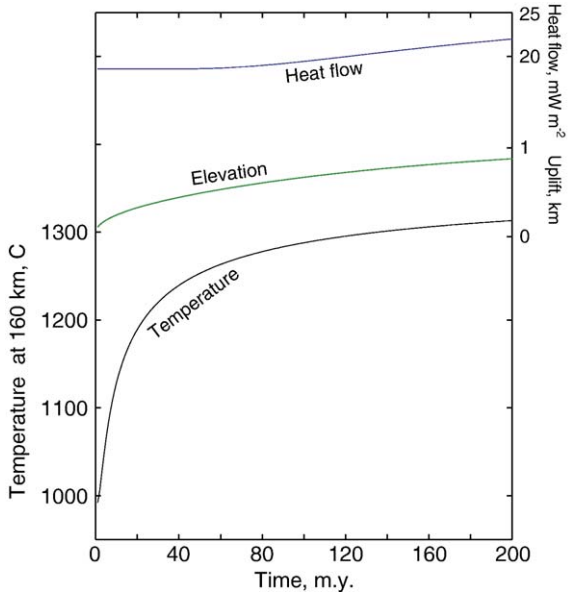

Fig. 16. Model starts with a conductive geotherm between 1300 °C at 180-km depth and 0 °C at the surface. The temperature at 180-km depth is then kept at 1500 °C. The temperature at 160-km depth (where it might be recorded by xenoliths) changes quickly. Elevation changes gradually and surface heat flow changes very little.

lithosphere can produce temperature increases at a given depth to the temperature of plume material and uplifts over a kilometer.

Current xenolith and inclusion observations suggest but do not mandate plumes. “Smoking-gun” detection of a plume requires recognizing temperatures well above the MORB mantle adiabat. Otherwise, the alternative hypothesis that the lower lithosphere foundered and got replaced (or intruded) by underlying material at the MORB adiabat is viable. One needs to get xenoliths exhumed before ponded plume material has had a chance to cool or “ultra-deep” isolated inclusions in diamond that record the ascent of the plume and conditions within it.

3. Plumes beneath Antarctica?

Ice covers the rock geology of much of Antarctica. The number if any of plumes beneath the region is not evident. Yet enough is known to amass constraints and make a working hypothesis. I follow Ebinger and Sleep’s (1998) study of Africa and seek a hypothesis with one or two strong plumes where the plume material ponds and follows laterally over large distances (Figs. 2 and 17). This approach is more testable and relatable to lithospheric geology than one with many weak plumes. It provides a natural example suggesting the interaction of starting plume heads at mid-mantle depths.

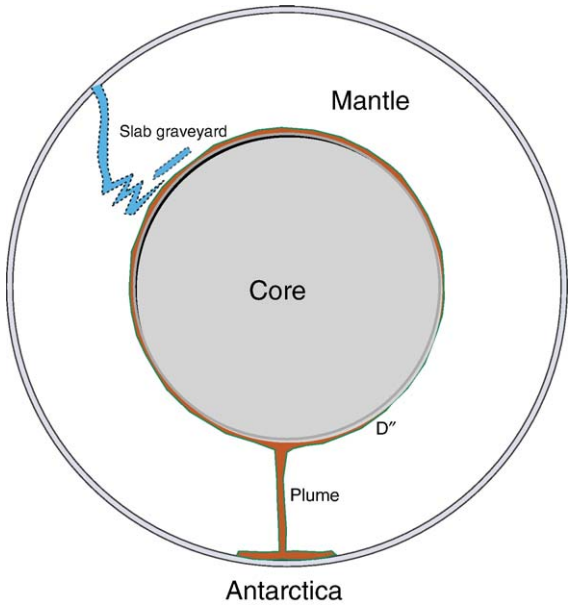

Fig. 17. Generic diagram at true scale with large plume beneath Antarctica. It is fed by a thin D″ layer. Slab graveyards exist elsewhere in the lower mantle.

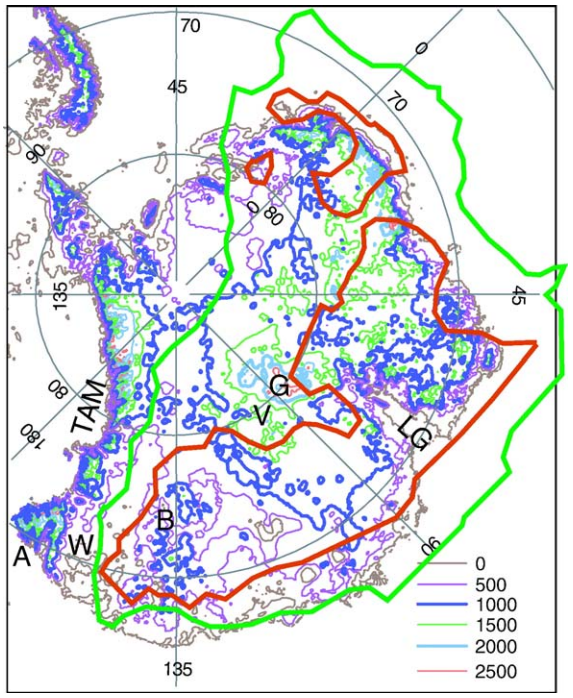

Fig. 18. Equivalent rock elevation map of East Antarctica. The contours in meters are the sum of the bedrock elevation plus (0.92/3.4) times the ice thickness of the BEDMAP data (Lythe and Vaughan, 2001). The thick red and green lines are the 220 and 150-km lithospheric thickness contours of Morelli and Danesi (2004), respectively. The corridor of thin lithosphere would tend to channel material from a plume in the Gamburtsev Mountains (G) or the Vostok highlands (V) toward the Transantarctica Mountains (TAM) where it would cascade across at rift. Lambert Graben extends (LG) from the coast to the north toward the Gamburtsev Mountains. The Adare Peninsula (A) is the northern end of the Transantarctic Mountains and Victoria Land. The difference in elevation between the Wilkes subglacial basin W and the Belica subglacial highlands (B) may owe to differences in erodability.

I keep place names to a minimum and spell them out in the text. Antarctica consists of the East Antarctic craton (Fig. 18) and more geologically active regions of West Antarctic (Fig. 19). The Transantarctic Mountains divide the two areas. They began as a break-up margin of East Antarctica in the late Precambrian and became an active margin in the Cambrian (Rowell et al., 2001; Wysoczanski and Allibone, 2004; Goodge et al., 2004). Most recently, rifting occurred along the edge of the Ross Sea, forming the current edifices. Passive margins bound the rest of East Antarctica. West Antarctica consists of accreted terranes.

Mt. Erebus is the only officially active volcano on the Victoria Land coast of the Ross Sea (LeMasurier and Thomson, 1990). Given the sampling problem in this remote region and my interest in the long term, the dormant and inactive volcanoes in their complication are relevant. Extensive land volcanism occurred in Victoria Land and Marie Byrd Land. Related volcanism occurred in Ellsworth Land (Hart et al., 1995). Gaussberg at the eastern margin of East Antarctica is an isolated edifice. There may well be volcanism within the Ross Sea and the West Antarctic Rift south of Marie Byrd Land. Winberry and Anandaknishnan (2004) contend that this volcanism is minor. Behrendt et al. (2004) use magnetic anomalies to suggest that the ice in the Ross Sea and West Antarctic Rift covers numerous late Cenozoic volcanic edifices. Balleny Islands, Scott Island (Fig. 20), and Peter I Island (Fig. 21) are young volcanic edifices on oceanic crust. Subduction-related regions of the Palmer Peninsula are beyond the scope of this paper.

I begin with Marie Byrd Land as it is the most straightforward place to postulate an active plume tail. I then move to East Antarctica, which is cloaked by ice. I briefly discuss volcanic edifices outside these regions to dynamically link them together.

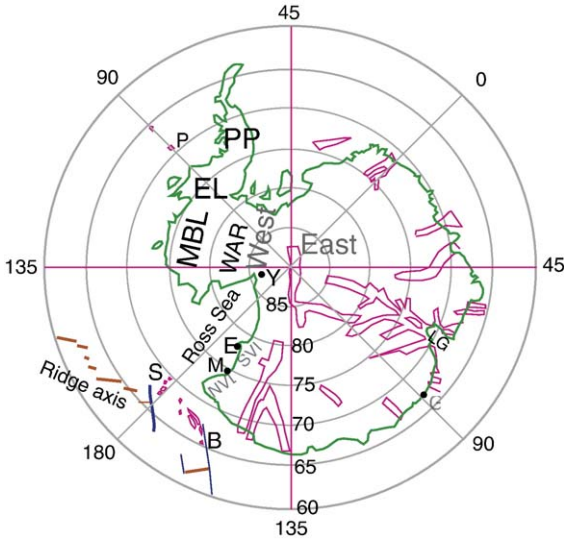

Fig. 19. Map of Antarctic and the surrounding ocean basin. Rifts beneath East Antarctica compiled by Sengör and Natal'in (2001). Oceanic islands include: Peter I (P), Scott (S), and Balleny (B). Gaussberg (G) is an isolated young edifice. Mountain Melbourne (M), Erbus (E), and Mount Early (Y) are volcanic centers along the Transantarctic Mountains (TAM). Magmatism at ~50 Ma occurred along the Lambert Graben (LG) but is poorly exposed. Rifted crust underlies the Ross Sea and the West Antarctic Rift (WAR) south of Marie Byrd Land (MBL). Magmatism began in Victoria Land at ~48 Ma. I divide the region into Northern (NVL) and Southern (SVL) Victoria Land around Mount Melbourne. Intraplate volcanism occurred in Ellsworth Land (EL). Subduction-related magmatism in the Palmer Peninsula (PP) is beyond the scope of the paper.

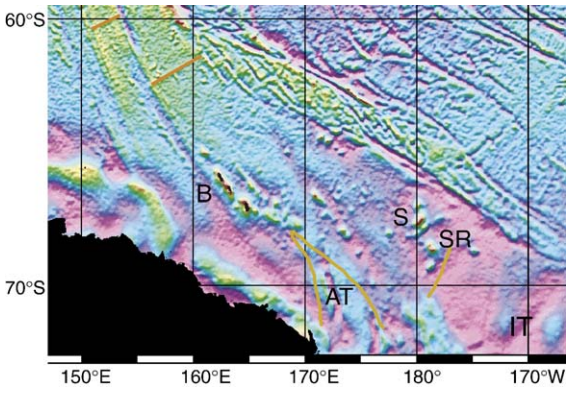

Fig. 20. Gravity of the seafloor around the Balleny (B) and Scott (S) Islands (Sandwell and Smith, 1997). The Balleny group lies on a flow line parallel to the Balleny fracture zone. The Adare trough (AT) is crust formed on a spreading center than extended south into the Ross Sea. The Scott rift (SR) is a break-up boundary with the young crust to the northeast. The Iselin trough (IT) is an abandoned spreading center.

3.1. Marie Byrd Land hotspot and the Ross Sea area

Winberry and Anandaknishnan (2004) review the evidence for the Marie Byrd Land hotspot. A 550-by-1000 km-wide dome rises to greater than 2700 m above sea level. Yet this region has only 25-km-thick crust. The West Antarctic Rift to the south of Marie Byrd Land has ~19 km thick crust. Xenolith data indicate that the lithosphere in the block dates back to ~1.2 Ga and that the geotherm is too hot for garnet-bearing mantle xenoliths (Handler et al., 2003). Some tomographic data show locally low seismic velocities in the upper mantle beneath the dome but not the more rifted region to the south (Ritzwoller et al., 2001; Sieminski et al., 2003; Shapiro and Ritzwoller, 2004). Morelli and Danesi (2004) show a general region of low seismic velocities including Marie Byrd Land, the Ross Sea, and the West Antarctic Rift.

The relative timing of crustal thinning and magmatism points to plume involvement. Rifting occurred in the Cretaceous between 105 and 85 Ma (Fitzgerald, 2002). Cenozoic extension is associated with the formation of oceanic crust at a spreading center in the Adare trough (Fig. 20) from 43 to 27 Ma (Cande et al., 2000; Stock and Cande, 2002; Cande and Stock, 2005, Müller et al., 2005). It is associated with extension along the East Antarctic margin of the Ross Sea (Fitzgerald, 2002). Magmatism has occurred in Marie Byrd Land since ~30 Ma (e.g., Hart et al., 1997). Strike-slip motion along with continental fragments on the Australia plate continued off northernmost Victoria Land until ~33 Ma (Stock and Cande, 2002; Cande and Stock, 2004, 2005; Hill and Exon, 2004) (Fig. 22).

The most active region on the Ross Sea coast of Victoria Land is the Mount Melbourne area south to around Erebus. The area has a long complex history. Magmatism in northern Victoria Land began at 48 Ma and continued to in their region of study until 18 Ma (Rocchi et al., 2002a, 2005). The Ross Sea coast has remained active until 1 Ma in Northern Victoria Land (Nardini et al., 2003). Dated rocks in Southern Victoria Land range from 24 Ma to the present (Rocchi et al., 2002a, 2005). Large intrusive complexes in Northern Victoria Land formed between 26 and 31 Ma (Rocchi et al., 2002b). Mount Early at the southern end of activity is ~16 Ma (LeMasurier and Thomson, 1990).

That is, the occurrence in time of magmatism correlates poorly with tectonics. Extension had run most of its course in the rifted area to the south in the West Antarctic Rift before intraplate magmatism began in Marie Byrd Land. Most of the extension along Victoria Land occurred before magmatism at 48 Ma and volcanism continued after East and West Antarctic became one plate at 27 Ma. An angular unconformity at ~24 Ma off shore of Southern Victoria Land demarcates the end of extensional tectonics (Hamilton et al., 2001). Neither did the end of transform tectonics in Northern Victoria Land at ~33.5 Ma stop magmatism. I agree that feeble tectonics that persisted after 27 Ma in Victoria Land (Rocchi et al., 2002a, 2005; Nardini et al., 2003) did modulate the local distribution of magmatism as did older structures.

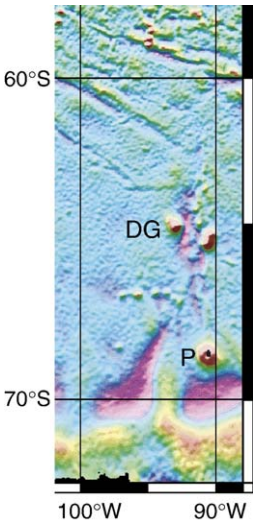

Fig. 21. Gravity of the seafloor around Peter I Island (P) and the De Gerache seamounts (DG) (Sandwell and Smith, 1997). The gravity low marks a poorly understood discontinuity in plate age. The young side is to the east. The continental margin is at the southern end of the map.

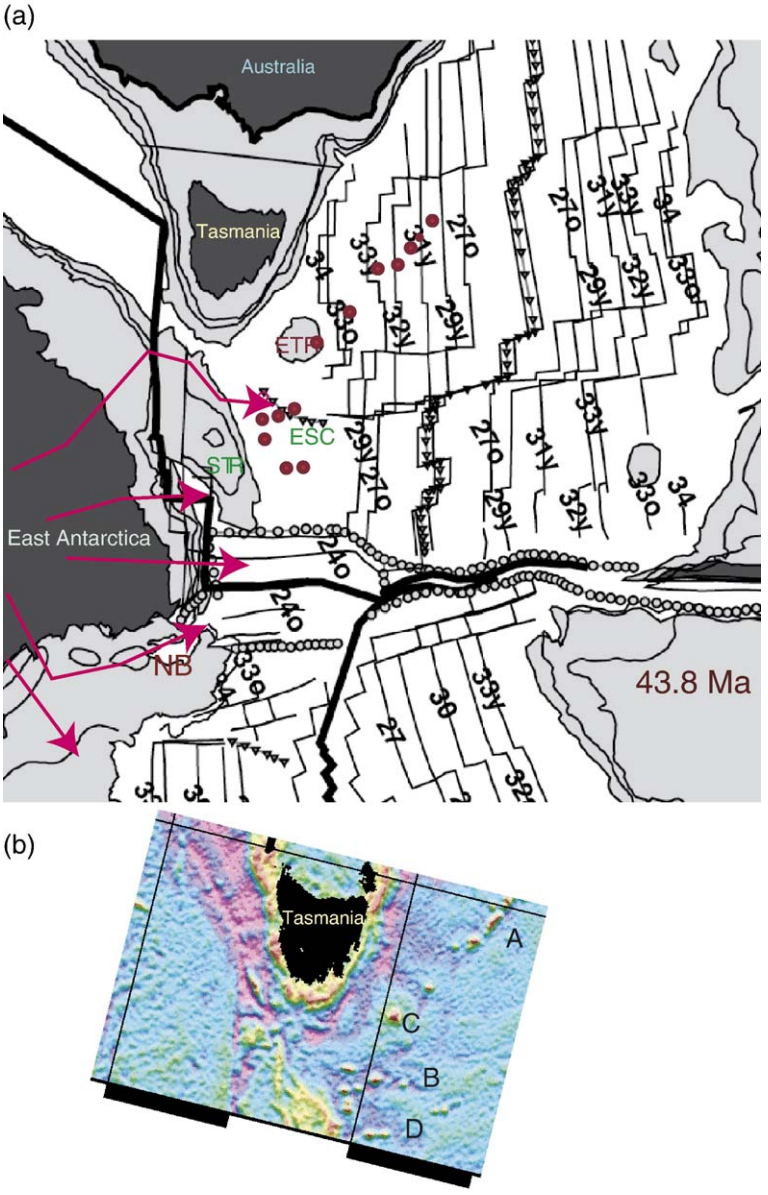

Fig. 22. (a) Map of magnetic isochrones, plate boundaries, and continental positions at 43.8 after Fig. 3c of Cande and Stock (2004) is modified to illustrate the plume hypothesis. I orient the map that fracture zones are "north–south." Current land is black, submarine continental crust is grey, and oceanic crust is white. Plume material flows from thick lithosphere beneath East Antarctic toward thin lithosphere (red arrows). It follows thin lithosphere north of the South Tasman Rise (STR) to form seamounts (red dots) along the passive margin and the extinct spreading center (ESC). It flows into the pull-apart south of the South Tasman Rise and across the transform passive margin. Flow beneath the Northern Basin (NB) may have formed thick transitional crust in that region. The East Tasman Rise (ETR) and seamount group to the northeast are not obviously associated with spreading plume material. (b) Gravity map around Tasmania from Sandwell and Smith (1997). Seamount group B is associated with the extinct spreading center. It and group D to the south show some tendency to align either along the passive margin or perpendicular to it. The seamount group A aligns with Cascade Seamount (C) on the East Tasman Rise.

All this suggests that the plume material ponded and produced magmatism in a region where the lithosphere was already thin. It cascaded from thick to thin lithosphere. The tomographic data and uplift suggest that the plume under Marie Byrd Land. Buoyant plume material from a plume outside this region would be expected to pond beneath the thinner lithosphere of the West Antarctic Rift and the Ross Sea. The Victoria Land magmatism may owe to a plume in that region or the flow of plume material

from thick East Antarctic lithosphere to thin West Antarctic lithosphere (Fig. 22).

3.2. East Antarctica

Thick glaciers cover East Antarctica except for coastal exposures and a few nunataks. Geologists deduce the crustal structure by comparing the geology of formerly contiguous parts of India, Australia, and Africa (Fitzsimons, 2003; Harley, 2003) and by examining detritus derived from the area (Rowell et al., 2001; Wysoczanski and Allibone, 2004; Goodge et al., 2004). Neither approach is ideal. For example, some of the detritus came from continental blocks that have since rifted away. Here we are after generalities. The gross age of stabilization is relevant to whether one expects chemically buoyant or ordinary mantle lithosphere beneath the region. There are younger Proterozoic to reactivated Archean regions so both are expected, but where beneath the ice is uncertain.

The age of the latest significant tectonism is relevant to where plume material might pond beneath thin lithosphere. The Lambert Graben system cuts from the coast to the Transantarctic Mountains (Fig. 19). It has a complex history (Lisker et al., 2003). The graben was first active in the Permian and Triassic. It then was a failed plated boundary in the Early Cretaceous separation of India from Antarctica. Glacial erosion of the sedimentary rocks in the graben has cut a deep subglacial valley (e.g., Taylor et al., 2004). I expect that the lithosphere beneath the graben was thinner than that beneath its immediate surroundings in the Tertiary before plumes impinged. Sheraton (1983) reports ~50 Ma alkalic lavas from the northern end of the graben.

Tomography (Fig. 18) shows thick lithosphere beneath East Antarctica and thin lithosphere beneath West Antarctica (Ritzwoller et al., 2001; Sieminski et al., 2003; Shapiro and Ritzwoller, 2004; Morelli and Danesi, 2004). The escarpment in lithospheric thickness follows the edge of the Ross Sea near the Transantarctic Mountains. All the late Cenozoic volcanism, except Gaussberg, occurs above lithosphere thinner than 150 km (Morelli and Danesi, 2004). The structure beneath East Antarctica is poorly resolved. Ritzwoller et al. (2001) and Shapiro and Ritzwoller (2004) do not show any. Sieminski et al. (2003) show velocity variations within East Antarctica at 200-km depth with a low-velocity east of the Vostok highlands. Morelli and Danesi (2004) resolve a reentrant of thin lithosphere from the eastern head of the Lambert valley through the Gamburtsev Mountains, the Vostok highland toward the East Antarctic margin near the Pole (Fig. 18). I use this study as in my figures as these authors processed their data specifically for lithospheric thickness. I acknowledge that it is at the limit of resolution. A lithospheric slope of the craton in the opposite direction would send plume material away from the Ross Sea margin.

As in Marie Byrd Land, topography constrains tectonic processes, given that erosion is occurring. The ice-free elevation of the Gamburtsev Mountains is over 2000 m and the nearby Vostok highlands are over 1500 m. These regions are too broad and too far away from the Lambert Graben to be rift-flank features. They are the prime suspects for a plume location.

3.3. Marine volcanic edifices and Gaussberg

Feeble offshore volcanic edifices in the ocean basin near the Ross Sea and Ellsworth Land make some lists of hotspots. These include the Balleny Islands and Scott Island (Fig. 20) and Peter I Island (Fig. 21). I include Gaussberg in this discussion even though it is on the continent. I do not present a Gaussberg chart because there are no notable offshore edifices in the region. All these edifices have been the subjects of limited geological study.

There are no convincing hotspot tracks in the ocean and the marine edifices have feeble volcanism. Attempts at tracking involve large gaps. For example, Lanyon et al. (1993) link the Balleny hotspot to the East Tasman Plateau and the Marie Byrd Land Hotspot to the initiation of spreading in the Tasman Sea. Hill and Exon (2004) discuss the problems of Balleny and prefer a location east of the South Tasman Rise. Storey et al. (1999) track a plume from just south of New Zealand to Erebus and have a second plume active since 30 Ma in Marie Byrd Land. Hart et al. (1995) note the lack of track problem when they suggest that Peter I is underlain by a plume. Rather I relegate Balleny, Scott, Peter I, and Gaussberg to secondary hotspots from the lateral flow of plume material toward thin lithosphere from beneath Antarctica or non-plume volcanism associated with cracks.

Physically, plume material flows laterally from thick lithosphere to thin lithosphere because it is buoyant. The base of the lithosphere is an upside-down drainage pattern (Albers and Christensen, 2001). Pressure-release melting in the plume material is most voluminous where the material cascades over escarpments in lithospheric thickness.

The Balleny Islands lie on the young side of the Bellany Fracture Zone and northwest of the end of the Adare trough (Fig. 20). They show evidence of relatively recent volcanic activity. The rocks are alkalic

(Green, 1992), but no radiometric ages are available (LeMasurier and Thomson, 1990).

The Balleny edifices are reasonably associated with the lateral flow of plume material from beneath the Ross Sea area, following a flow line toward the ridge axis. Tomography detects the hot upper mantle in the expected region from the northern Ross Sea along the Balleny fracture zone to the South Tasman Rise (Danesi and Morelli, 2000). Rocchi et al. (2005), however, conclude that this feature is evidence against the existence of plumes in general.

Secondary hotspots of this type are common in the ocean basins (Morgan, 1978). The Euterpe chain north of Hawaii is an example where the plume track is nearly perpendicular to the flow lines (Kopp et al., 2003). Thick lithosphere west of the Balleny fracture zone may have acted as a dam. Moving upstream, an extinct spreading center is within the Adare rift. The relatively thin lithosphere in that region may have acted as a funnel for buoyant plume material.

Scott Island is seaward on the young side of the Scott rift, an intraoceanic ridge-jump margin formed at ~61 Ma (Cande et al., 2000; Stock and Cande, 2002). About 50 km of extension occurred in the Iselin trough south of the Scott rift at about this time. The flat-topped island is obviously eroded. Other than the geomorphic inference of late Tertiary, there are no constraints on its age (LeMasurier and Thomson, 1990).

The Scott edifices show features expected from lateral flow. The Iselin trough to the north is a funnel, though not as well oriented as the Adare trough. All the edifices are on the young side of the Scott rift, a possible place for a cascade. The trend deviates to the east from a flowline. This takes it closer to thinner lithosphere.

Peter I Island is on the young side of a discontinuity in plate age (Eagles et al., 2004). It is either an extinct region of minor plate convergence (Eagles et al., 2004) or a later tensional feature (Udintsev et al., 2002). Much of the volcanism is clearly young (LeMasurier and Thomson, 1990; Prestvik and Duncan, 1991). A 13-Ma K–Ar date by Bastien and Craddock (1976) is problematic. Udintsev et al. (2002) regard it as real. Prestvik and Duncan (1991) attribute it to excess Ar. There are also young volcanic cones on the adjacent seafloor (Udintsev et al., 2002).

The De Gerlache seamounts straddle the gravity anomaly north of Peter I Island (Hagen et al., 1998). The eastern seamount is ~21 Ma. These guyots were beveled by erosion and are now deeper than 350 m.

Peter I and the DeGerlache seamounts lie along a plate-age and lithospheric thickness discontinuity. There are no obvious flowline features. They can equally well be attributed to cracks or lateral flow of plume material.

A group of seamounts occurs north of Marie Byrd Land. The largest seamount is a guyot ~1500 below the waves (Melisssa J. Feldberg, Wesleyan University Bachelor's thesis and 2005 personal communication, Steve Cande. personal communication 2005). Given the time to subside, this seamount group is probably ~61 Ma and associated with the demise of a spreading center (Stock and Cande, 2002). This group is too old to be relevant to the present volcanism in Marie Byrd Land.

Gaussberg is a young volcanic cone on continental lithosphere just off the coast. Dated lavas are ~50 ka (Tingey et al., 1983). This volcano erupted lamproite (Salvioli-Maiani et al., 2004), a rock indicative of cratonal thickness lithosphere. The magma is volatile-rich. It may have carried mantle xenoliths capable of giving the geotherm, but none have been reported. Any related edifices are covered with ice or eroded. Without mantle xenoliths, I do not have good explanation for this feature.

3.4. Plumes, lateral flow, and mid-mantle dynamics beneath Antarctica

I agree that a hypothesis involving only cracks in the lithosphere that let magma out is tempting for Antarctica (Rocchi et al., 2002a, 2005). This review is on plumes and their possible geological effect. I intend to illustrate the consequence of lateral flow of plume material beneath the lithosphere and the dynamics of starting plume heads in the mid-mantle. The buoyant plume material ponds within closed thin regions of the lithosphere. It tends to thin non-buoyant platform lithosphere. My objective is to make a self-consistent hypothesis on the dynamics of Antarctica that is subject to further scrutiny. Ice cloaks key areas, particularly in East Antarctica.

I also suggest that a more complicated mid-mantle fluid dynamic process may be relevant. Plumes start out with a massive head fed by a tail conduit. The head ponds at the base of the lithosphere and spreads laterally. Geologically, it produces a brief period of radial dike swarms, flood basalts, and mafic intrusions. Thereafter, the tail conduit leaves a plume track on the plate. Starting plume heads interact when they are nearby in the mantle (Schubert et al., 2004). Flow driven by their ascent causes them to entrain each other. Approaching plume heads might merge leaving a head with two tails. When the combined head reaches the surface, two nearby plume provinces start at about the same time.

It is useful to mention real features in terms of fluid dynamic hypotheses. Antarctica is a logical choice for paired plumes given its Cenozoic history. It has not escaped me that East Africa and Afar may be a similar pair of hotspots that started at about the same time.

Following this approach, I select two plumes within elevated regions, an indication of buoyant plume material and recently thinned lithosphere at depth. I place a strong "Vostok" plume somewhere beneath the Gamburtsev Mountains and Vostok highlands. I locate the other plume beneath Marie Byrd Land. The latter is conceivably a secondary hotspot from flow of buoyant plume material from Vostok. The converse is not. Plume material cannot flow against buoyancy from thin West Antarctic lithosphere to thick East Antarctic lithosphere. Similarly, plume material from near Erebus cannot flow to thick lithosphere beneath East Antarctica.

The sequence of events starts in the deep mantle. Well before 50 Ma, a mantle plume head starts to ascend toward Marie Byrd Land. The tail conduit provides a modest flux of material to the head. Ascent is slow. Later a more vigorous plume head starts to ascend toward Vostok. The large flux from its tail enlarges its head. It approaches the depth of the Marie Byrd Land plume head. The plume heads then interact, approaching each other (Schubert et al., 2004). They join into one large head then impinges on the base of the lithosphere at ~48 Ma. From this point on, we have a surface geological record.

The buoyant plume material beneath East Antarctic spread outward along the base of the lithosphere. It cascaded to thinner lithosphere along the Transantarctic Mountains. Pressure release melting led to magmatism in starting in Northern Victoria Land at 48 Ma (Rocchi et al., 2002a, 2005). Volcanism along the lithospheric escarpment eventually extended south to Mount Early.

The South Tasman Rise continental block was on the Australian plate by that time (Cande and Stock, 2004; Hill and Exon, 2004). The South Tasman Rise, however, was still across the Tasman fracture zone from Antarctic continental crust at 55 Ma. A wide zone of continental transform persisted at 43 Ma (Fig. 22) and did not clear until 33.5 Ma. I propose that the plume material spread across the continental transform fault and cascaded over the eastern passive margin of the South Tasman Rise. This provides an example of how few seamounts have reliable dates and how this makes analysis difficult.

I suggest that plume material cascaded over the eastern South Tasman passive margin. This produced volcanic edifices along this margin. The plume material continued to flow east beneath oceanic lithosphere producing submarine edifices. The timing of magmatism though poorly constrained (Hill and Exon, 2004) is compatible with this flow as is the widespread distribution of magmatism. Only Cascade seamount on the East Tasman Rise is dated by fossils as at least 37 Ma; the radiometric age of an igneous sample is 31.5–36 Ma (Quilty, 1997). Without age control, it is not clear whether this feature is associated with the seamounts east of the South Tasman Rise or a group of seamounts to the northeast.

The expected direction of flow of plume material beneath the oceanic lithosphere is uncertain as the position of crustal isochrons is poorly constrained. The conjugate flowlines are north–south parallel the margin. The situation east of the South Tasman Rise is likely to be more complicated (Steve Cande, 2005, personal communication). Royer and Rollet (1997) place an extinct spreading center of about 66 Ma perpendicular to the margin. The edifices are in the gross position expected from spillage, that is near the extinct spreading center. There is a weak tendency for edifices to align perpendicular to the South Tasman Rise margin.

Returning to East Antarctica, spillage of plume material along thin lithosphere beneath the Lambert Graben produced alkalic lavas at ~50 Ma (Sheraton, 1983). The exposed outcrop is only 8 km^2, but Ehrmann et al. (2003) speculate that abundant smectite in Miocene glacial detritus may have been sourced by widespread lavas that have been since eroded or are ice covered. Spreading in the Adare trough began at ~43 Ma (Cande et al., 2000; Stock and Cande, 2002). Gaussberg conceivably results from continued spillage in that direction.

Rifting along the Transantarctic Mountains in the Ross Sea and the West Antarctic rift took up the motion on land. Magmatism localized extension above pressure release melting in the cascade along the Ross Sea margin. Plume material ponded beneath the Ross Sea and West Antarctic rift added to the forces driving extension. Plume material flowed toward the spreading center in the Adare Trough along extending lithosphere in the Northern Basin (Fig. 22). The crust in the Northern basin is far too thick to be extended continental crust (Cande and Stock, 2005). Thick magmatic crust associated with plume material may underlie the Northern Basin (Müller et al., 2005).

The initial plume-head material produced a few 100 m of broad uplift within East Antarctica. Later the plume material from the tail thinned platform lithosphere beneath the Gamburtsev and Vostok regions producing the reentrant of thin lithosphere detected by Morelli and Danesi (2004) in Fig. 18. This resulted in higher uplift of these regions. The reentrant of thin

lithosphere channeled the plume material and concentrated magmatism within the currently active Mount Melbourne to Erebus region of Southern Victoria Land. Older structures have been recently reactivated in the Vostok region (e.g., Studinger et al., 2003), providing a hint on where a plume might be.

Models based on present topography indicate that continental glaciation initiated in the Gamburtsev Mountains (DeConto and Pollard, 2003). (In this model, the decline of CO_2 in the air over time was the primary trigger.) The onset of glaciation in East Antarctica at 34 Ma (e.g., Coxall et al., 2005) indicates that highlands in Gamburtsev and Vostok areas existed by this time. Glacial detritus carried by rivers to the mouth of the Lambert graben records earlier local glaciation and hence highlands (Strand et al., 2003). These sediments are between 34 and 37 Ma (Macphail and Truswell, 2004). This is a minimum age for the initiation of local glaciers. The basal sample of the unit is barren of fossils. It lies unconformably on Cretaceous sediments.

The Marie Byrd Land Plume was active by 30 Ma. Its material spread into Ellsworth Land and beneath the West Antarctic rift. The timing of volcanism after most of the extension is the strongest evidence for a plume in this region (Winberry and Anandaknishnan, 2004).

Overall Antarctica illustrates that we are still ignorant of shallow geological processes over much of the Earth's surface. We have a lot of detail in selected locations with wide gaps. Still the deep parts of the Antarctic plume hypothesis are testable independent of surface geology. In fact, the logistics of this remote sensing are probably easier than finding and dating magmatic centers below kilometers of ice. Lithospheric thickness and ponded plume material are detectable from seismology. Good data would be self-interpreting. I discuss plume conduits in the mid-mantle in the next section as a potentially definitive feature.

4. Plume conduits in the midmantle

Cartoon plumes are vertical cylindrical conduits ascending through much of the mantle (Fig. 17). This view is oversimplified, but quite useful for planning a seismic search. Mechanically, it leads to simple formulas that give qualitative insight into sophisticated fluid dynamic and seismic results.

I note that plumes may well interact with the 670-km transition zone in the mantle (Cserepes and Yuen, 2000). The negative Clapeyron slope of this phase change causes hot upwelling plume material to be locally denser than ambient mantle. Conversely, cold downwelling slabs locally become denser. This effect may well cause plumes to stop and temporarily pond at the transition zone. One deep plume may branch into several shallow plumes or plumes may begin at the transition. I acknowledge that these effects are possible in the Earth and that the behavior of slabs provides calibration. However, I do not discuss the process in detail because I have no useful way to simplify it with scaling parameters. I am aware of no full-mantle calculations of plumes penetrating the upper mantle that include realistic plates and slabs.

4.1. Heat and mass transfer in a tube

A simple plume consists of a hot core surrounded by a halo of slowly moving material warmed by the plume (e.g., Olson et al., 1993) (Fig. 23). Ordinary mantle exists beyond the halo.

Local buoyancy drives flow within the plume. Equivalently, the excess pressure within the plume is a small fraction of the excess pressure in an inviscid column, $\Delta\rho g M$, where $\Delta\rho$ is density difference between the plume material and ordinary mantle and M is the depth range across the mantle. A significant excess pressure would produce large uplift around the hotspot and a large geoid anomaly that are not observed (Sleep, 1990a,b).

The flux (volume per time) through the plume conduit is then

$$Q = \frac{\Delta\rho g \pi r_P^4}{8\eta_P} \tag{12}$$

where η_P is the viscosity of the plume material and r_P is the radius of the plume conduit. The viscosity and the radius are the least constrained parameters. For an example, I use a density contrast of 30 kg m^{-3} corresponding to a temperature contrast of 300 K at upper-mantle depth. The acceleration of gravity does not vary much from 10 m s^{-2} throughout the mantle. I use a high viscosity that might be appropriate for the deep lower mantle of 10^{20} Pa s. The volume flux for Hawaii, a vigorous plume, is 200 m^3 s^{-1} (Sleep, 1990a,b). The radius is then 114 km.

The plume radius narrows upward if the mass flux does not change much with depth because viscosity is depth dependent. For example, the radius for an upper mantle plume viscosity of 10^{17} is 20 km. Dynamic effects from the narrowing of the plume produce a long wavelength geoid anomaly, which is evident near Hawaii (Richards et al., 1988).

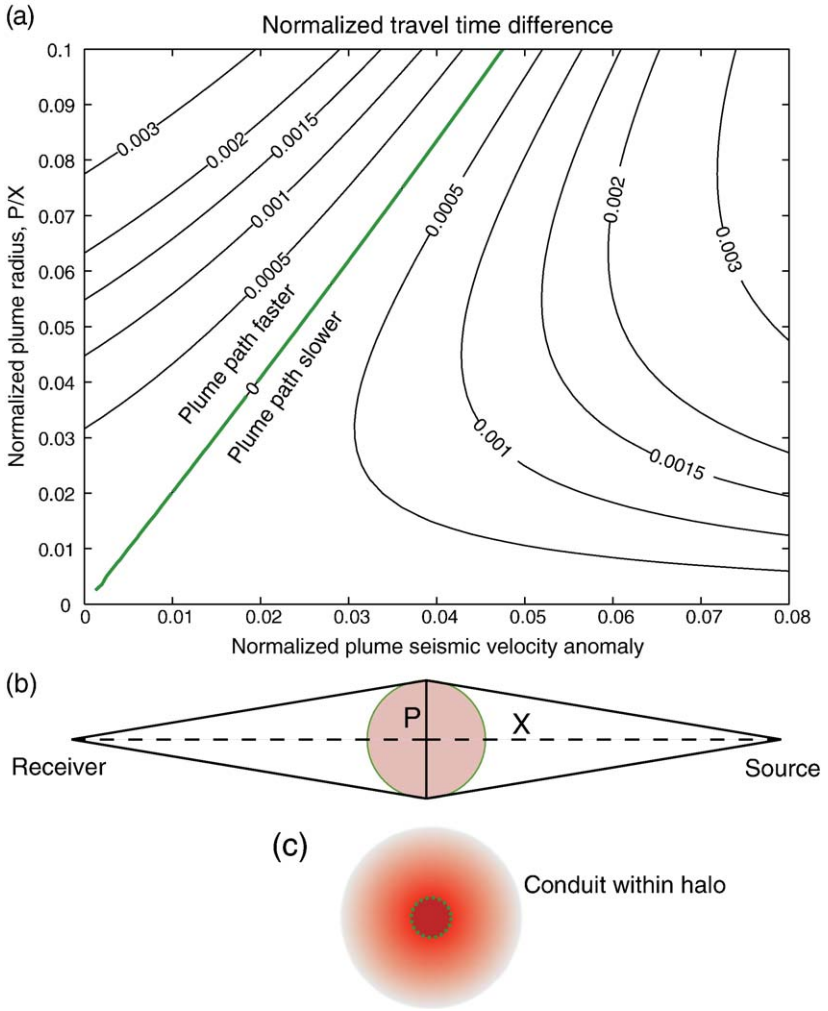

Fig. 23. (a) A difference in travel times illustrates the effects of plume conduits. (b) One path goes through a circular heterogeneity representing a plume and the other path goes around it. The times are normalized to the total travel time on the path of length X through normal mantle. The plume radius is P. (c) The circular homogeneous region in the model represents a plume conduit (dashed circle) within a fuzzy thermal halo.

Simple heat and mass transfer theory does not adequately constrain the radius of the halo around plume conduits (see Olson et al., 1993). Naively, the conductive halo should widen convectively proportionally to the thermal diffusivity times the square root of the age of the conduit. As plumes last ~100 m.y., like oceanic lithosphere, this scale distance is on the order of 100 km. However, inflow of material to the plume tends to narrow the thermal halo. Loper and Stacey (1983) give a steady state solution for inflow, but this steady state cannot be approached in a finite time (Sleep, 2004). Olson et al. (1993) provide time-dependent axisymmetric numerical models and analytical scaling.

Fully three-dimensional hard-to-model processes affect plume tails. Flow in the mantle, including the return flow from subduction zones to ridge axes, advects plume tails causing them to tilt (Steinberger, 2000; Steinberger et al., 2004). The tilted conduit buoyantly ascends though the surrounding mantle and convects internally entraining normal mantle (Richards and Griffiths, 1989). Tilted plume conduits may branch sending up new vertical plumes stems (Whitehead, 1982).

4.2. Seismic search for plume conduits

Gathering these gleanings, I appraise search for a simple vertical plume conduit. I expect that the radius to the edge of the halo is around 200 km in the lower mantle and somewhat over 100 km in the upper mantle. That is, it is comparable to the width of slabs, which gives some encouragement. However, plume conduits

are tubular not tabular features. They are also regions of low seismic velocity unlike slabs.

It is harder to find seismically slow features than fast ones with conventional travel-time seismology. Seismic stations typically record the first arrival in their bulletins, which is easiest to measure. This convention makes it difficult to detect isolated regions of low seismic velocity.

To illustrate the expected effects, I project the cross section of the plume including the conduit and halo and the ray path onto a plane. I let the plume and the surrounding mantle have different constant seismic velocities (Fig. 23). I center the plume so I can treat just half the path. Overall, these simplifications avoid obscuring the basic geometry with complicated algebra and ray tracing.

Tomograms often express seismic velocity variations as fractional deviation from the mean at some depth. I follow that convention in this example, but use dimensional quantities in equations. First the expected travel time over half the path if no plume were present is

$$t_0 = \frac{X}{V_0} \tag{13}$$

where X is the distance from the source to the plume axis and V_0 is the seismic velocity through ordinary mantle. A possible diffracted raypath bypasses the plume. Its travel time is

$$t_D = \frac{\sqrt{X^2 + P^2}}{V_0} \tag{14}$$

where P is the radius of the plume conduit. Assuming with justification for the lower mantle that the plume radius is a small fraction of the path length, the ratio of the two travel times is

$$\frac{t_D}{t_0} \approx 1 + \frac{P^2}{2X^2} \tag{15}$$

where the second term on the left is the fractional delay of the longer path. The direct ray goes through the center of the plume. Its travel time is

$$t_C = \frac{X - P}{V_0} + \frac{P}{V_P} \tag{16}$$

where V_P is the seismic velocity of the plume. This ray can be the first arrival if the velocity contrast between the plume and the ordinary mantle is small or the plume radius is large. Fig. 23 gives the difference between the two travel times.

As an example, I consider a path through the deep mantle where X is 4000 km. I let the radius P be 200 km. The normalized radius is thus 0.05. The path that bypasses the plume is the first arrival when the velocity contrast is greater than 2.3%. In this case, one cannot determine from the first arrival alone whether the velocity contrast is greater than 2.3%. The bypassing ray arrives 0.125% slower than a reference ray through normal mantle. In terms of the full time for a P-wave, this is delay is 0.85 s out of ~680 s, which is measurable but not easily resolved from other effects along the path.

The situation improves for stations near the upper part of the plume conduit. For example, consider teleseismic arrivals beneath Iceland or Hawaii. Then X is ~1000 km and the path through the plume arrives faster than the bypassing path if the fractional velocity change is less than 10%, keeping P at 200 km.

Modeling resolution improves if one accounts for diffraction, akin to the healing of an ocean wave after it passes through the pilings of a pier (Montelli et al., 2004; Hung et al., 2004; cf., van der Hilst and de Hoop, 2005). A seismic wave senses velocity variations around the theoretical ray path for a distance scaling to

$$F = \sqrt{\lambda X} \tag{17}$$

where λ is the wavelength and X is the half path length to the station or source whichever is closer. The Fresnel zone is a limit to resolution by travel times and geometric rays. It is significant in the deep mantle. For example, a 1-s P-wave in the lower mantle has a wavelength of ~10 km. Letting X again be 4000 km, the resolution is 200 km. A 10-s wave has 600 km resolution. Montelli et al. (2004) and Hung et al. (2004) account for this finite-frequency effect by measuring arrival times over a range of frequencies and mathematically inverting including diffraction.

4.3. Icelandic results

I discuss Iceland in some detail, as it is the *cause célèbre* for plumes not extending to great depth (Foulger et al., 2001; Foulger, 2002). In the Foulger et al. (2001) inversion, a columnar velocity anomaly extends down to ~450 depth with the P-wave velocity being up to 2.7% reduced and the S-wave velocity up to 4.9% reduced. This result is in basic agreement with the preliminary inversion by Allen et al. (1999) and the later inversion of Allen et al. (2002). Both these papers and Foulger et al. (2001) note the problems of resolution beneath 400 km depth and the problem of diffraction.

Hung et al. (2004) inverted seismic data from the same region using finite-frequency tomography. They confirm that the low-velocity column structure exists

down to 400-km depth and that resolution beneath that depth is poor. They show that ray-theory tomography underestimates velocity anomalies. Their preferred P-wave and S-wave velocity perturbations are 3.5% and 6.2%, respectively.

The lack of resolution below 400-km depth in this case occurs because of the less than optimal distribution of sources and receivers (Hung et al., 2004). At teleseismic distances, natural earthquake sources provide measurable signal. For the most part, these are limited to plate boundaries. For logistical reasons, the receivers around Iceland are on land. The net effect that few observed rays passed through the plume beneath 400-km depth and those that did also passed through the shallower low-velocity anomaly.

To be useful for geodynamics, seismic velocity anomalies need to be converted into variations of temperature and composition. Formally, I express the conversion as the first terms of a Taylor series,

$$V(T,z,C) = V_0(T_0,z,\Gamma_0) + (T-T_0)\frac{\partial V}{\partial T} + (\Gamma-\Gamma_0)\frac{\partial V}{\partial \Gamma} \tag{18}$$

where V is a seismic velocity, T is potential temperature that remains constant on an adiabat, z is depth, the single variable Γ compactly represents composition (really a vector with a component for each constituent), and the subscript zero indicates reference values.

In the case of an upper mantle problem like Iceland, one has reasonable constraints on the seismic velocity of ordinary mantle in the asthenosphere that is near the MORB adiabat. One does not know a priori that the plume has the same composition as the mantle, but unlike chemical cratonal lithosphere, high temperature is the key expected attribute of the plume. The temperature derivative is poorly constrained because small amounts of partial melt greatly slow down seismic waves. For example, Hung et al. (2004) infer temperature anomalies within the axis of the Iceland plume of 250–350 K assuming that partial melting is unimportant and note that the actual effect of partial melting is poorly constrained.

4.4. Plume viscosity

Eq. (12) relates the plume flux, which is inferred from hotspot studies, with parameters obtainable from tomography. This let one solve for the viscosity within the plume conduit (Korenaga, 2005). This approach, however, is vulnerable to smearing associated with tomography.

To illustrate how the difficulty arises, I note that the actual buoyancy flux of an imaged plume is

$$B = \Delta\rho Q = \frac{\Delta\rho_P^2 g \pi r_P^4}{8\eta_P} \tag{19}$$

where the subscript P indicates the actual parameters. One measures the radius r_m of the tomographic plume anomaly and a seismic velocity contrast ΔV_m. One then assumes that the density contrast $\Delta\rho_\mathrm{m}$ is proportional to the seismic velocity contrast as in Eq. (18). This step is problematic because the Taylor series coefficients in Eq. (18) are not well constrained. Tomography may thus image the broad warm conductive halo around the plume rather than the hot narrow low-viscosity conduit of the plume tail.

If one can in fact convert a velocity anomaly into a density anomaly and assign it to the flowing part of the plume, one obtains an estimate for the plume's viscosity

$$\eta_\mathrm{m} = \frac{\Delta\rho_\mathrm{m}^2 g \pi r_\mathrm{m}^4}{8B}. \tag{20}$$

This result is not in general the actual viscosity within the plume. The tomographic methods used by Montelli et al. (2004b) are complex enough the amount of smearing is not readily evident. I discuss two simple limiting cases. First, there is the high-frequency ray-theory limit where the travel time across the plume is resolved. This and the proportionality between density and seismic velocity imply that $\Delta\rho_\mathrm{m} r_\mathrm{m} = \Delta\rho_P r_P$. The measured viscosity then depends strongly on resolution

$$\eta_\mathrm{m} = \frac{\eta_P r_\mathrm{m}^2}{r_P^2}. \tag{21}$$

Second, the long-wavelength limit implies that the cross sectional anomaly is conserved $\Delta\rho_\mathrm{m}\pi r_\mathrm{m}^2 = \Delta\rho_P \pi r_P^2$, which yields the correct viscosity.

The Montelli et al. (2004b) methodology may be near the ray-theory limit (van der Hilst and de Hoop, 2005). The estimated viscosity in Eq. (21) then depends on the radius of the smeared tomographic anomaly squared. The conclusion of Korenaga (2005) that lower mantle plumes are very viscous is thus premature until the actual tomographic resolution and the dependence of density on seismic velocity are much better understood.

4.5. Worldwide results

Montelli et al. (2004b) obtained velocity anomalies for the entire mantle from finite frequency tomography. Her group resolved plumes under expected hotspots.

Ascension, Azores, Canary, Easter, Samoa, and Tahiti extend deep into the lower mantle. Hawaii may extend to great depths but is poorly resolved (Lei and Zhao, 2006). Iceland and Galapagos appear to extend down to at most 1000 km depth. Some plumes merge at depth or, more dynamically, fork on the way up. Azores, Canary, and maybe Cape Verde come from a common source. Ascension and St. Helena, and Crozet and Kerguelen are other forked pairs.

Yellowstone appears to be absent at depth. This may be an artifact as the high velocity of the Farallon slab may not be resolved from the low velocity of the plume. It is also conceivable that the plume impinges below on the slab (Geist and Richards, 1993). The cool slab material may cause the plume to bifurcate into the Yellowstone plume that ascends upward and a Cobb and Juan de Fuca plume that is deflected to the west beneath the slab.

Overall the results from Iceland and the global results are intriguing, frustrating, or tantalizing depending on one's mood and preconceptions on plumes. It is encouraging to proponents that seismologists find fuzzy indications of plumes beneath known hotspots. The structure is still not well enough resolved to infer dynamics from the details of the tomograms. Improvement is likely as the current techniques take advantage of only what are basically direct ray arrivals. There is unutilized signal from scattered arrivals and in the full waveform of the ray arrivals that might be used when denser receiver arrays come on line.

5. Plume sources and the base of the mantle

Dynamically, discussion of plumes should start with their source at depth. Plumes are the result of convection heated from below. A thermal boundary layer exists somewhere at depth (Fig. 24). Thicker places in the boundary layer become unstable and ascend as plumes. Stirring by plate motions including sinking slabs modulates the geometry of lower-mantle convection, but does significantly affect the global plume heat flow (Davies, 1993). Once free of the boundary, the plume material ascends, but its ascent has little effect on the rate that the boundary layer subsequently liberates hot material. This is the basic assumption of boundary-layer theories for parameterized convection. Specifically, the properties of the boundary layer determine the vigor of convection and to a large extent the tendency of convection to concentrate into tubular plumes.

The core–mantle boundary is clearly hotter than the MORB adiabat and thus should heat convection from below. Mineral physicists indirectly constrain the

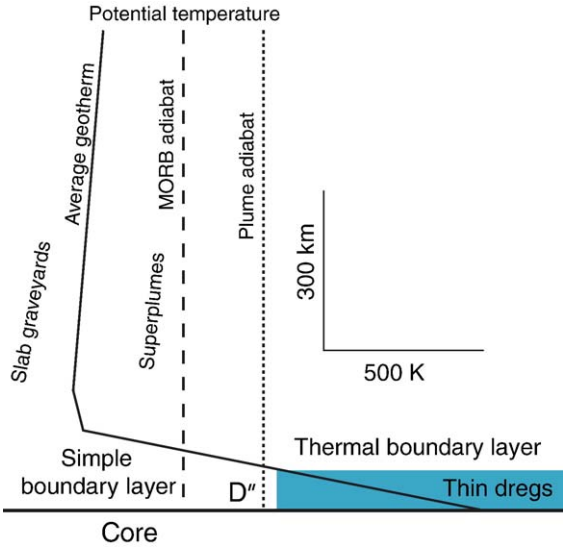

Fig. 24. Schematic diagram of the potential temperature in the lowermost mantle. A thin D″ layer is either a simple isochemical boundary layer left or a thin dregs layer beneath an isochemical boundary layer in ordinary mantle right. In the first case, the hottest material available to ascend has the core's temperature that is much hotter than the plume adiabat. In the latter, the temperature at the top boundary of the dregs is close to the plume adiabat. The average geotherm is subadiabatic. Slab graveyards are colder than the average. Superplumes are warmer than the average but cooler than the MORB adiabat.

temperature contrast. They extrapolate upward from the freezing temperature at the inner-core boundary. This is obtained from partly from theory (e.g., Laio et al., 2000); experiments are required for the effects of light alloying elements. The best estimate of the core–mantle boundary temperature is 3950–4200 K (Price et al., 2004). The MORB adiabat extrapolates to ~2700 K at that depth (e.g., Boehler, 2000), giving a temperature contrast of ~1400 K. This contrast occurs across the thermal boundary layer at the base of the ordinary mantle and perhaps across a chemical dense layer of "dregs" between the ordinary mantle and the core.

At present, seismologists provide only a fuzzy picture of the deep mantle. I piece together viable hypotheses using the seismic data, near surface information on hot spots, and simple dynamics including heat and mass balances. I intend to illustrate the basis of arguments without obscuring them in detail.

5.1. Mantle heat balance constraints

A key issue is that plumes are long-lived (over 100 m.y.) localized features. Hotspots are relatively fixed with respect to each other. Jellinek and Manga

(2004) thus distinguish plumes from feeble thermals that do not reach shallow depths. They note that gross properties of hotspots constrain models of their origin at depth.

Following their review, I start with plumes originating from a thermal boundary layer directly heated by the core (Figs. 17 and 24) to put surface constraints in context. The seismic layer D″ at the base of the mantle is about 100 km thick. As the density at that depth is about 5560 kg m^{-3}, there are 8.4×10^{22} kg of material in this layer.

I show that this region would be quickly depleted by plumes if not continually recharged. Earth scientists measure the vigor of plumes in terms of volume flux Q, buoyancy flux, $B\equiv\Delta\rho Q=\rho\alpha\Delta TQ$, and heat flux, $H\equiv\rho C\Delta TQ$. They define the temperature contrast ΔT with respect to the mantle adiabat. The physical constants are well constrained for the upper mantle. Studies of the uplift of hotspot swells give buoyancy flux (Davies, 1988; Sleep, 1990a,b). Studies of on-axis hotspots give volume flux (Sleep, 1990a,b; Schilling, 1991). Studies of melting at hotspots give an excess temperature of ~300 K.

The global estimates of plume flux by Davies (1988) and Sleep (1990a,b) are still used in recent discussions (e.g., Anderson, 2002; Jellinek and Manga, 2004; Nimmo et al., 2004). This does not imply great confidence. Rather, subsequent study has not improved the estimates within their uncertainty, ~±30%. I use Anderson's (2002) compilation of a global heat flux from plume tails of 2.3 TW. (TW is 10^{12} Watt; 1 TW produces a globally averaged heat flow of 1.96 mW m^{-2} at the Earth's surface). He adds 1.2 TW from Hill et al. (1992) for starting plume heads to get 3.5 TW. For a temperature excess of 300 K, the global mass flux is 10^7 kg s^{-1}, equivalent to a volume flux of 3000 m^3 s^{-1} in the upper mantle. This would deplete D″ in 270 m.y. It would turn over the whole mantle in 12.7 billion years. That is, extrapolating back to the early Earth a significant fraction of the mantle has been through plumes.

The need for recharge implies that the material in plumes previously downwelled into the deep mantle. This thermal effect of this process can be viewed in two equivalent ways. The average geotherm in the mantle well above D″ is subadiabatic (Fig. 24) or that cool "dead" slab material must be heated back to the MORB adiabat before it can be further heated to become a plume. Part of this heating may occur by weak thermals so explicitly including them counts their effect twice. The temperature deficit of the downwelling material and the temperature excess of plumes are comparable so both heat budget items are about 3.5 TW (see Anderson, 2002; Labrosse, 2002; Nimmo et al., 2004, for reviews). The net heat out of the core is thus ~7 TW. Bunge (2005) and Mittelstaedt and Tackley (2006) obtain similar results with the total heat flux greater than 3 (rather than 2) times that surface plume heat flux.

5.2. Core heat balance constraints

A parallel approach is to deduce the heat that comes out of the core. The magnetic field indicates that the core convects and hence is essentially at the adiabat gradient for molten iron with some lighter alloyed elements. The conductive heat flow along the adiabatic gradient is significant because metallic iron is a good conductor of heat

$$q = k\left(\frac{\partial T}{\partial z}\right)_S = \frac{k\alpha T}{C_P}, \tag{22}$$

where T is absolute temperature and C_P is specific heat at constant pressure. The thermal conductivity and the specific heat are the most uncertain parameters. Labrosse (2003) tabulates 20% and 10% uncertainties, respectively. Recent published estimates of the total conductive heat flux from the core are similar. Anderson (2002) gives a preferred global estimate of 6.8 TW; Nimmo et al. (2004) give 6.0 TW.

The heat to drive the convection that produces the magnetic field is less certain with estimates ranging from trivial to larger than the conductive heat flux. Christensen and Tilgner (2004) predict a modern amount of 0.2–0.5 TW by scaling from dynamo models. That is, the total heat from the core is ~7 TW. This is, close to what I cited for heat coming out of the mantle.

The source of the heat within the core is problematic. Specific heat from cooling the core, latent heat from freezing the inner core, and radioactive heat from potassium decay are the usual suspects (e.g., Nimmo et al., 2004). I return to potassium decay later because it is poorly constrained.

It is easy to obtain the cooling rate of the core if there are no heat sources in it. The specific heat of the core is ~850 J kg^{-1} K^{-1} (Labrosse, 2003). As the mass of the core is $\sim2\times10^{24}$ kg, cooling of the core by 100 K per billion years provides 5.4 TW of heat flow. Specific heat from cooling of the core can supply the observed heat flux of ~7 TW if the cooling rate is ~130 K per billion years. Latent heat is equivalent to the specific heat from cooling core material about 700 K (Labrosse, 2003). However, it is a modest budget item because the inner

core is only 5% of the mass of the whole core. For example, freezing the entire inner core in the last billion years would provide 1.9 TW.

5.3. Seismology, superplumes, D″, and dynamics

Seismologists obtain P-wave velocities, S-wave velocities, and densities in the lower mantle. The lower mantle (~2200–2800 km depth) consists of broad regions (superplumes) of low seismic velocity beneath hotspots and broad regions of high velocity where slabs have accumulated. The resolution is not uniform with the southern Indian Ocean being the least sampled region (Schubert et al., 2004). Hotspots occur preferentially above regions of low S-wave velocity. They are rare in regions of slab accumulation. Notably, the edges of the low S-wave velocity regions are sharp, that is, having high lateral gradients of S-wave velocity (Ni and Helmberger, 2003, Thorne et al., 2004). Hotspots are actually more concentrated over the high gradient regions than there are over the regions of the lowest S-wave velocity. The superplume regions may be denser than their surroundings (Ishii and Tromp, 2004). However, seismic data do not resolve any systematic global density excess in the deepest 500 km of the mantle (Masters and Gubbins, 2003).

If correct, the sharp gradients at its edge and higher density are obvious properties of a thick chemically dense region of dregs at the base of the mantle. Fluid dynamic models show that convection sweeps dense dregs into piles at the upwellings (Nakagawa and Tackley, 2004a). Moderately dense regions may form blobs that ascend somewhat like in a lava lamp. Plumes arise from the top of the blobs.

Seismologists also obtain reflection coefficients of the core–mantle boundary and the S-wave velocity of the lowermost mantle (Garnero and Lay, 2003; Lay et al., 2004). High velocities occur where slabs have gone down. A very low seismic velocity layer exists at the base of the mantle beneath regions of hot spots. It is frequently anisotropic. It is most evident beneath hotspots.

A phase change probably occurs at 2700 km depth (Nakagawa and Tackley, 2004b). The net effect is to destabilize convection by increasing buoyancy of hot regions. This tends to lead to smaller numerous plumes. This complication needs to be included in numerical models, but does not play an obvious role in the hypotheses that I discuss.

Available seismic data still lack resolution to be self-interpreting. It is possible to make several coherent hypotheses. I find it convenient to discuss them separately, as different aspects of the dynamics and the data relate to each one. I retain the widely used term superplume without any mechanistic implication.

5.4. Thin D″ within isochemical mantle

The D″ layer may represent a simple thermal boundary layer above the core within isochemical mantle (Fig. 24). This is the simplest hypothesis to evaluate and hence the easiest one to find wanting. Its failings introduce the strengths of models involving chemically dense dregs. In this hypothesis, current tomography data resolve only lateral temperature variations, not variations with depth from an adiabat. The lower mantle above D″ consists of slab graveyards that are cooler than the mantle adiabat, superplume regions that are warmer than the average geotherm but cooler than the MORB adiabat, and regions of inner the average temperature between them. I begin with what can be made consistent before going into the problems.

Superplumes simply indicate an absence of dead slabs within regions that have had hundreds of million years to heat up from radioactive decay and heating from below. These mechanically stable superplumes are passively displaced as more slabs settle into graveyards. For this to happen, the lower mantle needs to be quite viscous. Otherwise the dead slabs would spread out laterally to form a layer beneath the more buoyant superplume material.

Poorly resolved narrow plume tails within the superplumes may contribute to their low seismic velocity (Schubert et al., 2004). The thermal halos of these plumes gradually heat superplume volume.

Kinematic and dynamic difficulties result if one contends that superplumes are somewhat buoyant relative to the MORB adiabat. The volume (and mass) of the superplume regions is much larger than that of D″ so they cannot be easily recharged. Their volumes are larger than the flux of plumes over the ~200 m.y. period that plate motions evolve.

In addition, buoyant superplumes lead to an unattractive special time in history situation. A significant fraction of the deep lower mantle including that under Africa and the South Pacific consists of superplumes. Once detached from the base of the mantle, large buoyant regions ascend. (Note that the Stokes' law velocity depends on radius squared.) To exist now, the superplume regions would have had to just recently become buoyant with respect to the upper mantle. It would be surprising if superplumes on each side of the Earth became buoyant at the same time.

Dynamical issues arise from the heat balance across an isochemical boundary layer. First, the observed temperature contrast of plumes, ~300 K, is much smaller than the ~1400 K contrast between core and mantle on the MORB adiabat. Plumes result from instability in a fluid with strongly temperature-dependent viscosity (e.g., Olson et al., 1993). The hottest and least viscous region of the basal mantle flows laterally to supply the plume. This hot material then upwells within the tail conduit. The temperature of the material that actually upwells is close to the maximum temperature at the core–mantle boundary by an amount scaling with the temperature T_η to change viscosity by a factor of e in Eq. (1). As at least 2 orders of magnitude of viscosity difference must exist across the boundary layer to get a plume in the first place, one would expect the temperature difference to between plume and MORB adiabat to be ~1400 K, rather than the observed ~300 K. Vigorous plumes do not cool on the way up as the surface area of cylindrical conduits is small. For example, Olson et al. (1993) calculate that material within the Hawaiian plume could ascend through several mantle depths before significantly cooling.

Difficulties arise with the thermal history of the core. In the past, the core was hotter, implying that convection and the cooling rate were faster than today. One cannot expect simple models to represent the extreme aftermath of the Moon-forming impact. Still, one can reject situations that cannot be stably extrapolated back to reasonable temperatures within the early Earth.

Two modes of isochemical convection are possible above the core (Solomatov and Moresi, 2002; Ke and Solomatov, 2004). Plumes represent broad-scale convection. Starting with the mantle above the boundary layer, material sinks into the boundary layer, gets heated by the core, flows lateral to the plume source, and upwells. Flow occurs both in the plume material and the ordinary mantle. In analogy to Eq. (2), the heat flow carried by plumes is

$$q_P = Pk\Delta T\left[\frac{\rho g\alpha\Delta T^3}{\kappa\eta_E}\right]^{1/3} \tag{23}$$

where ΔT is the temperature contrast between the core and the MORB adiabat that drives flow and P is a dimensionless constant of the order of 1. A simple form for the effective viscosity for plume convection is the product

$$\eta_E \equiv \eta_B^a \eta_M^b; \quad a+b=1 \tag{24}$$

where η_B is the viscosity of the mantle at the core–mantle boundary temperature, η_M is the viscosity at the MORB adiabat, and a and b are positive dimensionless constants.

Small-scale convection may occur within the boundary layer (Solomatov and Moresi, 2002; Ke and Solomatov, 2004). In that case a thin thermal boundary layer exists at the base of a near isothermal boundary layer (Fig. 25). Stagnant-lid convection occurs at the top of the isothermal region. As with stagnant-lid convection at the base of the lithosphere, the temperature contrast occur the rheologically active boundary layer scales to T_η in 1. A conductive thermal gradient occurs between the rheological boundary layer and the nearly isothermal mantle above it. As is Eq. (2), the stagnant-lid heat flow is

$$q_{SL} \approx 0.5kT_\eta\left[\frac{\rho g\alpha T_\eta^3}{\kappa\eta_C}\right]^{1/3} \tag{25}$$

where the viscosity is that at the core–mantle boundary temperature (Solomatov and Moresi, 2002, Eq. (23)).

The two modes of convection interact (Solomatov and Moresi, 2002; Ke and Solomatov, 2004) (Fig. 25). The top of the small-scale convection moves upward consuming the isothermal mantle. This thickens the low viscosity channel within the boundary layer, making it easier for material to flow towards the plume. The broad-scale instability of plumes develops before stagnant-lid convection is well established if the viscosity contrast between ordinary mantle and mantle at the core temperature is less than a factor 10^4 (Solomatov and Moresi, 2002, Eq. (17)). Plumes can develop in the presence of stagnant-lid convection, but the theory has not progressed to a point that provides the heat flow in this combined mode (Ke and Solomatov, 2004).

I construct thermal histories of the core to illustrate the essence of the problem with an isochemical mantle. I begin using Eq. (23) assuming that the plume mode is important. The variables that may change significantly with time are the effective viscosity and the temperature contrast. The other variables are uncertain at lower mantle depths, but they are not expected to change much over time. I calibrate the model so that it gives the current heat loss of 7 TW from the core. The heat flow in the past is then using Eq. (1),

$$q_P = q_{now}\left[\frac{(T_C - T_M)}{(T_C - T_M)_{now}}\right]^{4/3} \exp\left(\frac{a(T_C - T_{C_{now}})}{3T_\eta}\right) \times \exp\left(\frac{b(T_M - T_{M_{now}})}{3T_\eta}\right), \tag{26}$$

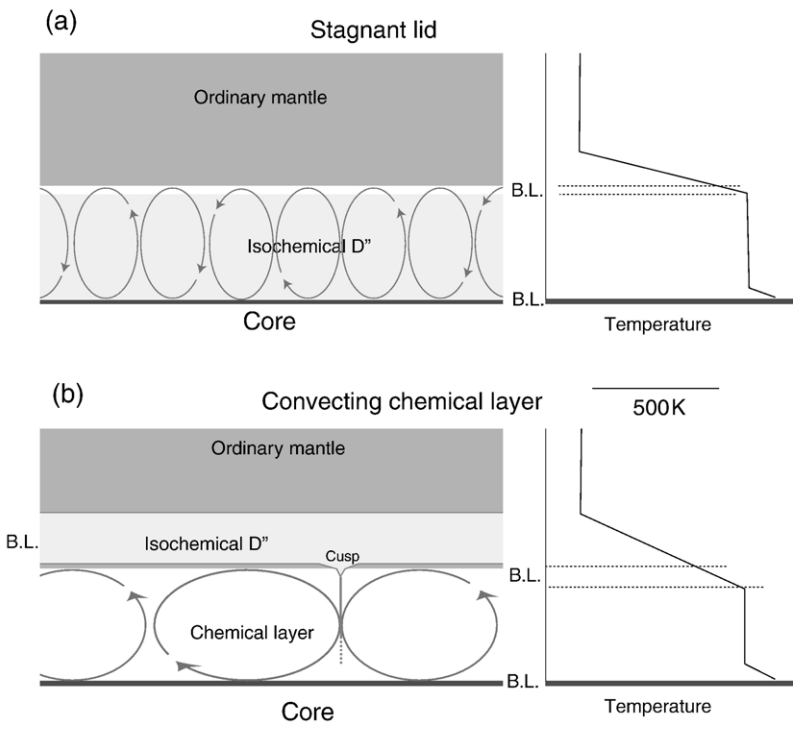

Fig. 25. Heat transfer issues arise if the D″ layer is quite fluid. (a) An isochemical layer convects vigorously as a stagnant lid beneath ordinary mantle. The convective region grows upward, forming a thick hot layer at nearly the core's temperature. (b) A fluid dregs layer convects internally. Most of the temperature contrast is in the isochemical boundary layer at the base of the ordinary mantle, not in the dregs. The dregs layer entrains wisps of the overlying mantle. This eventually causes it to lose its identity.

where T_C and T_M are the temperatures at the base of mantle and the MORB adiabat and the subscript now indicates current values.

The mantle cools over time mainly from plate tectonics. I let its cooling rate be 50 K per billion years (Abbott et al., 1994; Galer and Mezger, 1998) as it is much better constrained than the temperature in the core. In a full calculation (e.g., Nimmo et al., 2004), this cooling rate is calculated from the heat balance in the mantle. The cooling rate of the core assuming no radioactive heat generation or latent heat is proportional to the heat flow,

$$-\left(C_P\frac{\partial T_C}{\partial t}\right)\left(\frac{4\pi r_c^3\rho}{3}\right)=4\pi r_e^2 q_P, \tag{27}$$

where r_e is the radius of the core. The current cooling rate of the core is ~130 K per billion years. This is faster than the mantle has cooled. All three terms (26) thus have decreased with time. This implies the cooling rate was faster in the past.

If one integrates Eq. (27) backward in time, the result becomes unacceptably unstable if viscosity is too strongly temperature dependent. Strictly, one should use the stagnant-lid heat flow (25) which is even more strongly dependent on the temperature of the core when the viscosity contrast is greater than 10^4. This hastens the time back to the instability.

I let T_η be 100, 150, and 300 K to illustrate the effect of that parameter. The viscosity contrasts across the current 1400 K boundary layer are 1.2×10^6, 1.1×10^4, and 106, respectively. The latter model represents the minimum viscosity contrast across the current thermal boundary layer to get plumes. I let the constants a and b be 1/2 for simplicity following Nimmo et al. (2004).

The core temperature decreases over the history of the Earth as expected (Fig. 26). The model with weakly temperature-dependent viscosity T_η=300 K integrates stably back in time. The viscosity contrast stays $<10^4$ within the plume regime. The model with T_η=100 K illustrates that models with strongly temperature-dependent viscosity cannot be integrated back in time over the age of the Earth. The model with T_η=150 K integrates but to high temperatures at the age of the Earth. One could construct a more sophisticated model had plume convection (23) for viscosity contrasts below

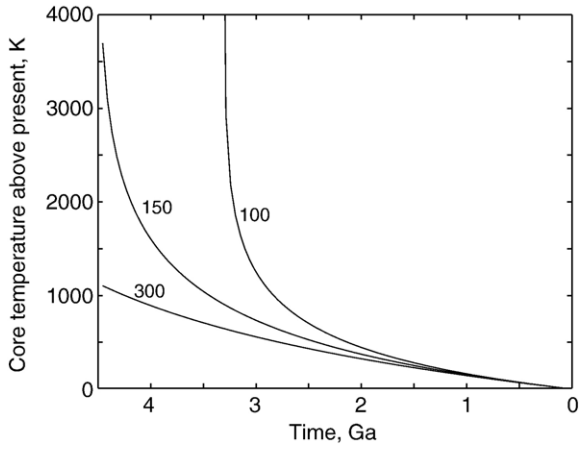

Fig. 26. Thermal histories of the core for various values of the viscous temperature scale T_η. The models are computed back in time starting from current conditions. The model with T_η=100 K cannot be extrapolated back to the age of the Earth.

10^4 and stagnant-lid convection (25) above that that had that property consistent with a hot core after the Moon-forming impact.

Although the temperature-dependence of viscosity at the base of the mantle is not well constrained, it is a material property not a free parameter. If the temperature dependence is strong, we can reject models with no core heat sources and isochemical mantle convection. Acceptable models where the core temperature does not change a lot can be obtained with potassium in the core providing an additional heat source (Nimmo et al., 2004). This is another essentially unconstrained parameter, but it is a measurable property once neutrino detectors sensitive to potassium decay are available.

5.5. Thin chemical D″

The difference between the temperature excess of plumes, ~300 K, and the temperature contrast between the core and the MORB adiabat, 1400 K, motives models with a chemical dense layer at the bottom of the mantle. Much of the temperature drop occurs within the chemical layer (Fig. 24). This leaves only a few 100 K for the basal boundary layer of the isochemical mantle, about right for the excess temperature of plumes. Thin and thick chemical layers have different kinematic implications. I discuss them separately, keeping to generalities.

The thin chemical layer is stably stratified with respect to but strongly affected by the overlying mantle. The chemical material is swept into piles at upwellings and displaced away from areas where slabs sink (Jellinek and Manga, 2004). Unless it is continually regenerated, say from oceanic crust in slabs, its existence faces three perils. It needs to avoid wholesale overturn into the ordinary mantle. That is, it needs to be stay denser than the overlying mantle when hot. Even if it is stable to gross overturn, flow entrains tendrils of dense material from cusps into the cores of plumes (Fig. 27). If the layer internally convects, downwellings at the top of the layer entrain ordinary mantle (Fig. 25). Over time this thickens the layer while reducing the density contrast with ordinary mantle. This may make the layer vulnerable to wholesale overturn. Radially symmetric numerical models (Lin and van Veken, 2006) resolve entrainment by the plume, but not entrainment of normal mantle into the dense layer. Chemical D″ needs to be 2–6% more dense than ordinary mantle to persist over geological time against entrainment in plumes (Sleep, 1988; Davaille, 1999; Davaille et al., 2002; Lay et al., 2004; Lin and van Veken, 2006, and references therein). How it got that way to begin with is beyond the scope of this paper.

Convection within chemical D″ should occur as rolls aligned along the flow direction toward plumes (Fig. 25). If vigorous, this convection would effectively entrain overlying mantle (Davaille et al., 2002). Vigorous convection would also transport heat effectively across chemical D″ reducing the temperature contrast across the layer. That is, the chemical layer needs to be both thick enough that a significant conductive temperature drop occurs across it but thin and viscous enough that it does not vigorously convect.

Dynamically the cusps on the top of the chemical layer keep plumes stable over long periods of time (Jellinek and Manga, 2004). This is a ready explanation

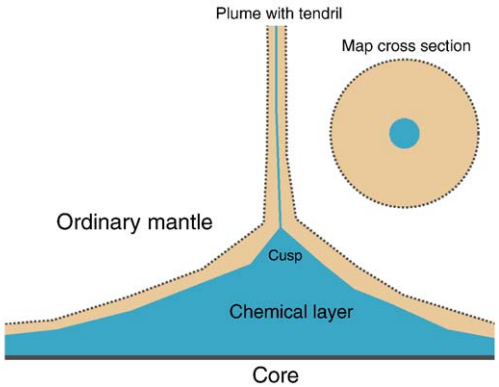

Fig. 27. Schematic diagram of entrainment of a dense chemical layer in the core of a plume conduit. A tendril of dense material arises from the cusp at the center of the upwelling. Given enough time and no replenishment, this process would remove the dregs layer.

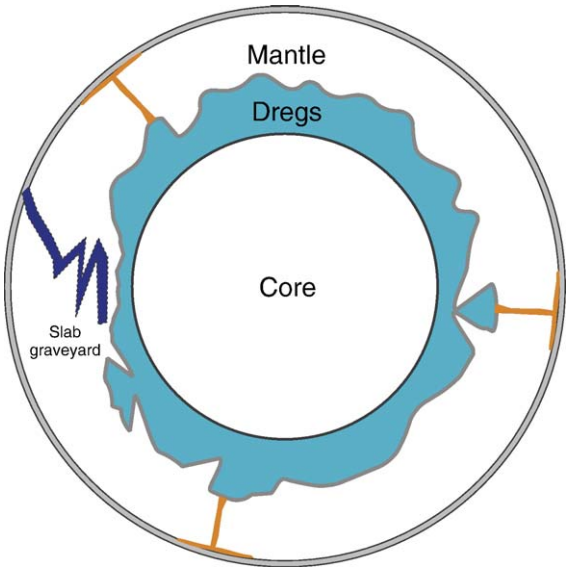

Fig. 28. Schematic diagram of convection with a thick dregs layer. Plumes arise from the centers and edges of upwellings of the thick layer. Blobs may detach from the layer. Slab graveyards displace the dregs.

for the fixity and longevity of hotspots. Convection in an isochemical fluid does not have this property.

Thin regions of very low S-wave velocity at the base of the mantle underlie regions with hotspots (e.g., Lay et al., 2004). High velocities occur where slabs have gone down (e.g., Garnero and Lay, 2003). The basal mantle tends to be anisotropic beneath hotspots as might be expected from material flowing laterally toward plumes.

These observations are evidence that a chemical layer exists at the bottom of the mantle (e.g., Lay et al., 2004). An iron-rich chemical layer melts at a lower temperature than ordinary mantle. The dense melt does not readily ascend into the overlying mantle. The layer is thickest away from slabs were the thermal gradient is lowest. Unfortunately the excess density of a thin layer cannot be easily resolved seismically.

5.6. Thick chemical lava lamp

The mantle may behave like a lava lamp with a thick dregs layer at the base of the mantle (Kellogg et al., 1999; Davaille, 1999; Davaille et al., 2002) (Fig. 28). The core heats the layer and buoyant regions upwell. They may sometimes detach as blobs. Plumes arise from the top and edges of upwellings and from the top of detached blobs if any exist. As with a thin chemical layer, cusps on the top of the chemical layer tend to keep plumes fixed (Davaille, 1999; Davaille et al., 2002). Large regions of the layer may become unstable at the same time, leading to pulsations like in a lava lamp (Le Bars and Davaille, 2004).

The great volume of the dregs layer protects it from losing its identity by mingling with the ordinary mantle over geological time. (Note that the lava lamps sold in curio stores have two immiscible fluids. Surface tension, which is negligible on the scale of mantle convection, prevents mingling.)

Superplumes are the upwellings of the hot dense layer into the normal mantle (Figs. 28 and 29). The layer is thinner beneath slab graveyards. The great volume of the layer gives some hope of detecting it seismically. As already noted sharp edges (Ni and Helmberger, 2003; Thorne et al., 2004) and excess density (Ishii and Tromp, 2004; cf. Masters and Gubbins, 2003) are positive evidence that these dregs exist. The layers existence is compatible with regions of low S-wave velocity at the base of the mantle as the partially molten region should be thickest away from slab graveyards.

Fluid dynamic models show that plumes should arise as expected above upwellings. Families of weaker plumes may arise from detached blobs (Nakagawa and Tackley, 2004a). The shape of the chemical upwellings depends on whether they are more or less viscous than their surroundings (McNamara and Zhong, 2004). Theory thus provides much information on the dynamics once the dregs layer and plume conduits are resolved. Right now we do not have good constraints

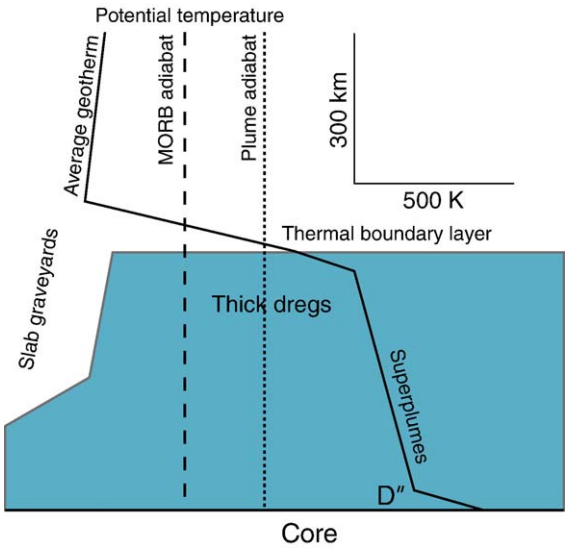

Fig. 29. The potential temperature in the lowermost mantle with a thick dregs layer. D″ is the temperature boundary layer at the base of the dregs. Superplumes are hot dense upwellings of the dregs. Slab graveyards locally displace the dregs. The isochemical boundary layer above the dregs feeds plumes.

on what the dregs should be like and how they might have formed to include in dynamic calculations.

5.7. Bottom line on the base of the mantle

Current seismic information and dynamics are compatible with plumes being generated at the base of the mantle, but we have no definitive evidence. Hotspots occur above low S-wave velocity regions in the deep mantle and away from high S-wave velocity slab graveyards. We suspect the superplume regions of low seismic velocity are hotter than their lateral surroundings, but we do not know whether they are chemically dense dregs.

The best estimates of the heat provided by the core and the heat taken up by plumes are in agreement. The cusps at the top of dreg piles tend to stabilize plumes. The existence of a dreg layer readily explains why the temperature excess of plumes ~300 K is much less than the temperature contrast between core and mantle ~1400 K. Beyond this, the dynamics are not well understood. Convection with a dreg layer is complicated and difficult to model without good seismic constraints.

6. Conclusions

The existence of plumes is controversial to some and old-hat to others 40 years after Wilson (1963) pointed out the existence of hotspots and 30 years after Morgan (1972) proposed the existence of mantle plumes. When Wilson published, seafloor spreading was primitive; subduction and transform faults were not yet on the horizon. Yet by 1967, when I attended a conference in Woods Hole, it was clear that much of the marine community acknowledged the overwhelming evidence for seafloor spreading. The whole of plate tectonics became widely accepted by 1970. The different fates of plates and plumes owes to dynamical complexity and logistics.

Hotspots, seafloor floor spreading, and full plate tectonics all began as kinematic theories. Wilson's (1963) statement proved prophetic with respect to plate tectonics. "The observations upon which to base such an analysis are abundant, but, until now, they have not proved diagnostic." He foresaw that physicists and geologists need only focus together on the appropriate scale. Magnetic stripes made seafloor spreading a record-producing process. Transform faults gave the geometry on a sphere. Deep focus earthquakes showed the reality of subduction.

At my first heavy exposure to seafloor spreading in 1967, it was clear that the marine scientists did not know how it worked. It did not bother them, as they were concerned with the validity of the geometrical hypothesis. Geometrical plate tectonics gives the first order effects on the Earth's surface with rigid plates and weak plate boundaries. One can reassemble continents. One can predict the age of the seafloor in a drill hole, the mechanism of a plate-boundary earthquake, and where deep earthquakes occur, all without knowing what drives motion. I had found an unpicked orchard of low-hanging dynamic fruit. The rigidity of plates lets one construct good thermal models of oceanic lithosphere, slabs, and ridge axes. The depth–age relationship of the seafloor was a prime result.

To be sure, the kinematic theory of plates was incomplete. Earth scientists have been busy since 1970. There were global kinematic unknowns at the time. Do slabs subduct into the lower mantle? How long ago did plate tectonics occur? What are the effects of the nonrigidity of plates? None of these bear on the essential validity of the surface hypothesis.

Wilson's (1963) intent was to show the movement of what is now called the Pacific plate. He needed only a source of heat at some depth that moved slowly relative to the surface plate. In fact, he placed the source within the core of a convection cell, not at the core–mantle boundary. Kinematic hotspot theory in fact works. The relative motion of the stronger hotspots is in fact small enough, that their fixity was a useful approximation in early plate reconstructions.

Morgan (1972) turned the kinematic hypothesis into a dynamic one with mantle plumes. The heart of the hypotheses lurks in the middle and deep mantle. He had to piece together what was going on by gleaning observations of the surface. The situation has improved considerably since 1972, but skeptics are justified in demanding deep evidence for a deep mantle hypothesis. The geologist, the seismologist, and the dynamicist still have great difficulty getting on the same scale, even though they recognize the need to do so.

Reversing the order of presentation in the paper, seismologists have published tantalizing tomograms of the lower mantle. Dynamicists have powerful computer codes. Yet these lines of attack have not convinced doubters. The difficulty is that the physical properties of the lower mantle, particularly the dependence of viscosity on temperature, pressure, and composition are not known independently. The fluid dynamicist needs to treat the Earth as a natural experiment to get reliable values. The seismic data are currently inadequate for this task. Not knowing whether the superplume regions are chemically denser than normal mantle does not help. The deep dregs layer (Kellogg et al.,

1999) and the core (Nimmo et al., 2004) remain potential "hidden" reservoirs for heat producing elements. Slight amounts of their entrained material provide free parameters for explaining the chemistry of ocean–island basalts.

Moving up to the mid-mantle, the first order behavior of flow in tubular plume–tail conduits is simple. Lateral flow into the conduit complicates the thermal halo. Conduits may branch or form at the expense of broader deeper upwellings. They may interact with slabs and with the 670-km phase change. Seismic data are beginning to resolve features in the expected places. This line of attack is most likely to be conclusive in the near future. The other aspects of the plume hypothesis then fall in place. Well-resolved conduits need sources at depth and places to impinge at the base of the lithosphere.

Unlike magnetic stripes, relevant evidence on surface hotspots is quite incomplete. I picked Antarctica as the worst case. The high elevation of East Antarctica is explained if a vigorous plume impinges beneath it. Lateral flow of the plume material may explain volcanism in West Antarctic, Peter I Island, Scott Island, and Balleny islands, and even the East Antarctic volcano Gaussberg. There is no definitive evidence from either seismology or geology for even the number of Antarctic plumes. Most of the region is covered with ice and the relatively well-exposed regions are often snow covered.

Xenoliths from the base of the lithosphere have the potential of recording mantle plumes in the past. The physics of the base of the lithosphere are not difficult, but obtaining thermal histories from xenoliths is. At present, one can see evidence of lithospheric heating and thinning, not direct evidence of hot plume material.

Overall, hotspots are a well defined, but complex attribute of the Earth. Their effects are three-dimensional and dynamic even at shallow depths. The plume hypothesis for the major hotspots has passed inspection where it has been testable. However, tests beyond the behavior of surface hotspots are at present cursory to tantalizing. Improved seismology is likely to become definitive on the question of existence of plumes in the mid-mantle. We really do not know how the deep Earth works. We need much more seismic data.

Acknowledgments

Gillian Foulger suggested forming additional testable hypotheses about plumes. Paul Tackley, Alan Cooper, Steve Cande, Joann Stock, and Melissa Feldberg promptly answered questions. This work was in part supported by the National Science Foundation grants EAR-0000743 and EAR-0406658.

Appendix A. Hotspots produced by plate drag

Shaw and Jackson (1973) suggested that drag on the base of moving plates causes hotspots. One cannot exclude this hypothesis wholly on energetic grounds. The available energy of shear strain heating is large. Physically, the dissipation number

$$N = \frac{\alpha g h}{C}, \tag{A1}$$

where h is the height of the convecting system, is the ratio the heat generated by dissipation to the total heat transmitted by convection. It is ~ 0.47 for whole mantle convection (van den Berg et al., 2002) and about half that from convection powered by radioactive heating of the mantle or cooling of the mantle over time. This fraction is large enough that shear strain heating may locally generate high temperatures in the Earth. It does that on fault planes during earthquakes.

There are two main difficulties with this mechanism as a way to produce hotspots. First hotspots occur on both slow and fast moving plates. They occur near ridge axes were the upwelling material is likely to be too fluid to act as an anchor. Second, a feedback mechanism limits frictional heating even beneath fast-moving plates. The region of high drag becomes more fluid as it heats up thus self-regulating shear–strain heating.

Shaw and Jackson (1973) address the latter problem for Hawaii by having material that delaminates from the base of the lithosphere act as anchors. This material is initially more viscous than ordinary mantle, so the issue is whether it can heat up above the ambient temperature of the mantle. This eventuality cannot be excluded, as convection is complicated. The relevant material properties depend on temperature, composition, and depth (e.g., van den Berg et al., 2002). So far, no one has developed a three-dimensional fluid dynamic model or even a good scaling argument that acts in this way.

Doglioni et al. (2005) present a variant of this hypothesis where the Earth's lithosphere rotates rapidly westward en masse. This modification addresses the issue of hotspots on slowly moving plates, but not hotspots at high latitudes where the rotation velocity is slow. Scoppola et al. (2006) discuss tidal torque as the driver for rapid >100 mm yr^{-1} westward drift.

Tides do in fact produce a torque on the lithosphere, but it is quite small equivalent to a global stress of 10^{-5} Pa (Jordan, 1974; Ranalli, 2000). The viscosity would have to be 10^{10} to 10^{11} Pa s for plates to move at

their typical rates. Scoppola et al. (2006) raise this viscosity to 10^{12} Pa s by arguing that Jordan (1974) neglected the effect of solar tides. This is still far below other estimates for the viscosity of the lithosphere.

Determination of the instantaneous torque on the Earth is complicated by glacial rebound. Good limits, however, exist for the long-term torque that is relevant to generation of long-lived hotspots. The torque over 4.5 Ga of the Earth's history cannot be greater than that to decelerate the Earth from a body at rotational instability to its present rate. One can safely discount multiple order-of-magnitude errors in tidal torque estimates.

Jordan's (1974) paper did not have its intended effect. Journals publish papers advocating tidal drive of plate motions almost every year. Arguments for tidal drive are qualitative and thus hard to appraise. For example, Scoppola et al. (2006) following Wang (1975) state that the effective viscosity for deformation by tidal torque is orders of magnitude lower than the effective viscosity for deformation by other processes because tidal stresses oscillate about the mean stress associated with torque. Wang (1975) notes that earthquakes are a nonlinear phenomenon. For example, a slight stress bias might cause west-dipping thrusts might fail more easily than thrusts dipping in other directions. This bias might in turn cause a net rotation of the lithosphere driven by buoyancy force associated with plates and slabs.

The effect of oscillating stresses is easily quantified. Substantial weakening does occur, but then the oscillations approach or exceed the mean stress (Weertman and Blacic, 1984). Mathematically, scalars suffice here to demonstrate the effect of small oscillating stresses because orders of magnitudes of weakening are needed for tidal torque to be important. The strain rate for power law creep is

$$\varepsilon' = \frac{\tau^n}{\eta \tau_{\mathrm{ref}}^{n-1}}, \tag{A2}$$

where τ is stress, η are the dimensions of viscosity, and τ_{ref} is a reference stress that I let be the mean ambient stress without loss of generality. The effective viscosity for the mean stress is then $\eta = \tau/\varepsilon'$. The effective viscosity of a small perturbation is

$$\eta_{\mathrm{s}} = \left[\frac{\partial \varepsilon'}{\partial \tau}\right]^{-1} = \frac{\eta}{n}. \tag{A3}$$

This effect may produce a factor-of-a-few difference between effective viscosities but not many orders of magnitude.

Coupling of convection energy with tidal torque may seem attractive. Tidal stresses do in fact modulate the occurrence of shallow thrust events (Cochran et al., 2004). These stresses, however, are small, 5×10^3 Pa for earth tides and 5×10^4 for tidal water loads, compared with tectonic stresses. Water loads, unlike torque, do not have a westward bias. They are orders of magnitude greater than mean stress from torque. Cochran et al. (2004) include the effect of oscillating stresses on fault rheology in their analysis. The net effect is to modulate the time of rupture over a day. Slip occurs in the direction determined by tectonic stress.

Returning to hotspots, Doglioni et al. (2005) use local high-stress asperities from tidally driven net rotation discussed by Scoppola et al. (2006) to produce hotspots. The combined numbers in the two papers by this group are not consistent unless a bias from tidal stress allows buoyancy forces to drive rapid net rotation. Doglioni et al. (2005) correctly show that combined with a net plate velocity of 200 mm yr^{-1} asthenospheric viscosity of 10^{20} Pa s suffices to generate modest excess temperatures. If tidal torque directly drives the rotation, the stress produces a torque and the area over which this stress acts need to be included in the linear global average viscosity for tidal rotation of 10^{12} Pa s of Scoppola et al. (2006). The total area over which this asperity can act is thus the area of the Earth, 5.1×10^8 km^2 divided by the ratio 10^{20} Pa s/10^{12} Pa s, that is, 5 km^2, which is too small to drive a hotspot. Jordan's (1974) estimate of the average viscosity to drive plates tidally is 2 orders-of-magnitude lower. This yields the tiny area of 0.05 km^2. Without detailed numerical calculations showing the contrary, I am highly skeptical of both direct and indirect tidal drive as a cause of westward drift and hotspots.

Net westward drift of the lithosphere is likely. This quantity is obtained directly from fluid dynamic models, which include plates, faults, and laterally varying viscosity. The observed drift of ~17 mm yr^{-1} is compatible with differences by continents and oceans (Ricard et al., 1991; Ranalli, 2000). It is in good agreement with the net motion of the hotspot frame relative to a frame with no net rotation. The predictions of full three-dimensional models can be compared with slabs dips, intraplate stresses, and plume conduits if these are well resolved. The asthenospheric viscosity may well be less than that of the rest of the mantle and have a significant effect on plate tectonics (Richards et al., 2001).

There are additional processes that weakly couple the rotation of the Earth to tectonics and produce stresses orders of magnitude greater than tidal torque.

The acceleration of gravity is greater at the pole than at the equator. Pole fleeing force arises because acceleration from rotation varies with elevation. The polar radius is less than the equatorial radius. The stresses from these effects are approximately the ellipticity, ~1/300, times the "ordinary" stresses driving convection.

Goldreich and Toomre (1969) describe a subtle rotational effect that has an observable effect on tectonics. The axis of maximum nonhydrostatic ellipticity in a somewhat fluid body aligns with the rotational axis. Equivalently, the maximum nonhydrostatic geoid is centered on the equator. Plate tectonic features that cause geoid highs, probably subduction zones and slab graveyards, are thus likely to be at low latitudes. The high viscosity of the deep mantle and the persistence of subduction zones stabilize the position of the excess bulge relative to geography (Richards et al., 1997).

References

Abbott, D.L., Burgess, L., Longhi, J., Smith, W.H.F., 1994. An empirical thermal history of the Earth's upper mantle. Journal of Geophysical Research 99, 13835–13850.

Albers, M., Christensen, U.L., 2001. Channeling of plume flow beneath mid-ocean ridges. Earth and Planetary Science Letters 187, 207–220.

Allen, R.M., Nolet, G., Morgan, W.J., Vogfjord, K., Bergsson, B.H., Erlendsson, P., Foulger, G.R., Jakobsdottir, S., Julian, B.R., Pritchard, M., Ragnarsson, S., Stefansson, R., 1999. The thin hot plume beneath Iceland. Geophysical Journal International 137, 51–63.

Allen, R.M., Nolet, G., Morgan, W.J., Vogfjörd, K., Bergsson, B.H., Erlendsson, P., Foulger, G.R., Jakobsdottir, S., Julian, B.R., Pritchard, M., Ragnarsson, S., Stefansson, R., 2002. Imaging the mantle beneath Iceland using integrated seismological techniques. Journal of Geophysical Research 107 (B12), 2325. doi:10.1019/2001JB000595.

Anderson, D.L., 2000. The thermal state of the upper mantle; no role for mantle plumes. Geophysical Research Letters 27, 3623–3626.

Anderson, O.L., 2002. The power balance at the core–mantle boundary. Physics of the Earth and Planetary Interiors 131, 1–17.

Bastien, T.W., Craddock, C., 1976. The geology of Peter I Island. Initial Reports of the Deep Sea Drilling Project 35, 341–357.

Behrendt, J.C., Blankenship, D.D., Morse, D.L., Bell, R.E., 2004. Shallow-source aeromagnetic anomalies observed over the West Antarctic Ice Sheet compared with coincident bed topography from radar ice sounding—new evidence for glacial "removal" of subglacially erupted late Cenozoic rift-related volcanic edifices. Global and Planetary Change 42, 177–193.

Bell, D.R., Schmitz, M.D., Janney, P.E., 2003. Mesozoic thermal evolution of the southern African mantle lithosphere. Lithos 71, 273–287.

Bleeker, W., 2003. The late Archean record: a puzzle in ca. 35 pieces. Lithos 71, 99–134.

Boehler, R., 2000. High-pressure experiments and the phase diagram of lower mantle and core materials. Reviews of Geophysics 38, 221–245.

Boyd, F.R., Gurney, J.J., Richardson, S.H., 1985. Evidence for a 150–200 km thick Archean lithosphere from diamond inclusion thermobarometry. Nature 315, 387–389.

Bunge, H.P., 2005. Low plume excess temperature and high core heat flux inferred from non-adiabatic geotherms in internally heated mantle circulation models. Physics of the Earth and Planetary Interiors 153, 3–10.

Cande, S.C., Stock, J.M., 2004. Cenozoic reconstructions of the Australia–New Zealand–South Pacific sector of Antarctica. The Cenozoic Southern Ocean: Tectonics, Sedimentation, and Climate Change between Australia and Antarctica. Geophysical Monograph Series, vol. 151. American Geophysical Union, Washington, D.C., pp. 5–17.

Cande, S.C., Stock, J.M., 2005. Constraints on the timing of extension in the Northern Basin, Ross Sea, preprint.

Cande, S.C., Stock, J.M., Müller, R.D., Ishiihara, T., 2000. Cenozoic motion between East and West Antarctica. Nature 404, 148–150.

Carlson, R.W., Moore, R.O., 2004. Age of the Eastern Kaapvaal mantle: Re–Os isotope data for peridotite xenoliths from the Monastery kimberlite. South African Journal of Geology 107, 81–90.

Carlson, R.W., Pearson, D.G., Boyd, F.R., Shirey, S.B., Irvine, G., Menzies, A.H., Gurney, J.J., 1999. Re–Os systematics of lithosphere peridotites: implications for lithosphere formation and preservation. In: Gurney, J.J., Gurney, J.L., Pascoe, M.D., Richardson, S.H. (Eds.), Proceedings of the 7th International Kimberlite Conference The J. B. Dawson Volume. Red Roof Design, Cape Town, pp. 117–124. 493 pp.

Christensen, U.R., Tilgner, A., 2004. Power requirement of the geodynamo from ohmic losses in numerical and laboratory dynamos. Nature 429, 169–171.

Cochran, E.S., Vidale, J.E., Tanaka, S., 2004. Earth tides can trigger shallow thrust fault earthquakes. Science 306, 1164–1166.

Courtillot, V., Davaille, A., Besse, J., Stock, J., 2003. Three distinct types of hotspots in the Earth's mantle. Earth and Planetary Science Letters 205, 295–308.

Coxall, H.K., Wilson, P.A., Pälike, H., Lear, C.H., Backman, J., 2005. Rapid stepwise onset of Antarctic glaciation and deeper calcite compensation in the Pacific Ocean. Nature 433, 53–57.

Cserepes, L., Yuen, D.A., 2000. On the possibility of a second kind of mantle plume. Earth and Planetary Science Letters 183, 61–71.

Danesi, S., Morelli, A., 2000. Group velocity of Rayleigh waves in the Antarctic region. Physics of the Earth and Planetary Interiors 122, 55–66.

Davaille, A., 1999. Two-layer thermal convection in miscible viscous fluids. Journal of Fluid Mechanics 379, 223–253.

Davaille, A., Jaupart, C., 1993a. Thermal convection in lava lakes. Geophysical Research Letters 20, 1827–1830.

Davaille, A., Jaupart, C., 1993b. Transient high-Rayleigh-number thermal convection with large viscosity variations. Journal of Fluid Mechanics 253, 141–166.

Davaille, A., Jaupart, C., 1994. The onset of thermal convection in fluids with temperature-dependent viscosity: application to the oceanic mantle. Journal of Geophysical Research 99, 19853–19866.

Davaille, A., Girard, F., Le Bars, M., 2002. How to anchor hot spots in a convecting mantle? Earth and Planetary Science Letters 203, 621–634.

Davies, G.F., 1988. Ocean bathymetry and mantle convection: 1. Large-scale flow and hotspots. Journal of Geophysical Research 93, 10467–10480.

Davies, G.F., 1993. Cooling the core and mantle by plume and plate flows. Geophysical Journal International 115, 132–148.

Davis, R.M., Griffin, W.L., O'Reilly, S.Y., McCandless, T.E., 2004. Inclusions in diamonds from the K14 and K10 kimberlites, Buffalo Hills, Alberta, Canada: diamond growth in a plume? Lithos 77, 99–111.

DeConto, R.M., Pollard, D., 2003. Rapid Cenozoic glaciation of Antarctica induced by declining atmospheric CO_2. Nature 421, 245–249.

Doglioni, C., Green, D.H., Mongelli, F., 2005. On the shallow origin of hotspots and the westward drift of the lithosphere. In: Foulger, G. R., Natland, J.H., Presnall, D.C., Anderson, D.L. (Eds.), Plates, plumes, and paradigms. Geological Society of America Special Paper, vol. 388, pp. 735–749.

Doin, M.-P., Fleitout, L., Christensen, U., 1997. Mantle convection and stability of depleted and undepleted continental lithosphere. Journal of Geophysical Research 102, 2771–2787.

Eagles, G., Gohl, K., Larter, R.D., 2004. High-resolution animated tectonic reconstruction of the South Pacific and West Antarctic margin. Geochemistry Geophysics Geosystems 7, Q07002. doi:10.1029/2003GC000657.

Ebinger, C., Sleep, N.H., 1998. Cenozoic magmatism throughout east Africa resulting from impact of one large plume. Nature 395, 788–791.

Ehrmann, W., Bloemendal, J., Hambrey, M.J., MCKelvey, B., Whitehead, J., 2003. Variations in the composition of the clay fraction of the Cenozoic Pagodroma Group, East Antarctica: implications for determining provenance. Sedimentary Geology 161, 131–152.

Feng, M., Assumpção, M., Van der Lee, S., 2004. Group-velocity tomography and lithospheric S-velocity structure of the South American continent. Physics of the Earth and Planetary Interiors 147, 315–331.

Fitzgerald, P., 2002. Tectonics and landscape evolution of the Antarctic plate since the break-up of Gondwana, with an emphasis on the West Antarctic Rift System and the Transantarctic Mountains. In Antarctica at the close of a millennium. Royal Society of New Zealand Bulletin 35, 453–469.

Fitzsimons, I.C.W., 2003. Proterozoic basement provinces of southern and southwestern Australia, and their correlation with Antarctica. In: Yoshida, M., Windley, B.F., Dasgupta, S. (Eds.), Proterozoic East Gondwana: Supercontinent Assembly and Breakup. Geological Society London. Special Publication, vol. 206, pp. 93–130.

Foulger, G.R., 2002. Plumes or plate tectonic processes. Astronomy and Geophysics 43, 19–23.

Foulger, G.R., Pritchard, M.J., Julian, B.R., Evans, J.R., Allen, R.M., Nolet, G., Morgan, W.J., Bergsson, B.H., Erlendsson, P., Jakobsdottir, S., Ragnarsson, S., Stefansson, R., Vogfjörd, K., 2001. Seismic tomography shows that upwelling beneath Iceland is confined to the upper mantle. Geophysical Journal International 146, 504–530.

Foulger, G.R., Natland, J.H., Anderson, D.L., 2005. Genesis of the Iceland anomaly by plate tectonic processes. In: Foulger, G.R., Natland, J.H., Presnall, D.C., Anderson, D.L. (Eds.), Plates, plumes, and paradigms. Geological Society of America Special Paper, vol. 388, pp. 595–625.

Galer, S.J.G., Mezger, K., 1998. Metamorphism denudation and sea level in the Archean and cooling of the Earth. Precambrian Research 92, 387–412.

Garnero, E.J., Lay, T., 2003. D″ shear velocity, anisotropy and discontinuity structure beneath the Caribbean and Central America. Physics of the Earth and Planetary Interiors 140, 219–242.

Geist, D., Richards, M., 1993. Origin of the Columbia Plateau and Snake River plain: deflection of the Yellowstone plume. Geology 21, 789–792.

Goldreich, P., Toomre, A., 1969. Some remarks on polar wandering. Journal of Geophysical Research 74, 2555–2567.

Goodge, J.W., Williams, I.S., Myrow, P., 2004. Provenance of Neoproterozoic and lower Paleozoic siliciclastic rocks of the central Ross orogen, Antarctica: detrital record of rift-, passive-, and active-margin sedimentation. Geological Society of America Bulletin 116, 1253–1279.

Griffin, W.L., O'Reilly, S.Y., Ryan, C.G., 1999. The composition and origin of sub-continental mantle. In: Fei, Y., Bertka, C.M., Mysen, B.O. (Eds.), Mantle Petrology: Field Observations and High Pressure Experimentation: A Tribute to Francis R. (Joe) Boyd. Geological Society, Special Publication, vol. 6, pp. 13–45.

Green, T.H., 1992. Petrology and geochemistry of the basaltic rocks from the Bellany-Is., Antarctica. Australian Journal of Earth Sciences 39, 603–617.

Griffin, W.L., O'Reilly, S.Y., Natapov, L.M., Ryan, C.G., 2003a. The evolution of the lithospheric mantle beneath the Kalahari Craton and its margins. Lithos 71, 215–241.

Griffin, W.L., O'Reilly, S.Y., Abe, N., Aulbach, S., Davies, R.M., Pearson, N.J., Doyle, B.J., Kivi, K., 2003b. The origin and evolution of Archean lithospheric mantle. Precambrian Research 127, 19–41.

Hagen, R.A., Gohl, K., Gersonde, R., Kuhn, G., Volker, D., Kodagali, V.N., 1998. A geophysical survey of the De Gerlache seamounts: preliminary results. Geo-Marine Letters 18, 19–25.

Hamilton, R.J., Luyendyk, B.P., Sorten, C.C., 2001. Cenozoic tectonics of the Cape Roberts rift basin and Transantarctic Mountains front, southwestern Ross Sea, Antarctica. Tectonics 20, 325–342.

Handler, M.R., Wysoczanski, R.J., Gamble, J.A., 2003. Proterozoic lithosphere in Marie Byrd Land, West Antarctica: Re–Os systematics of spinel peridotite xenoliths. Chemical Geology 196, 131–145.

Harley, S.L., 2003. Archaean–Cambrian crustal development of East Antarctica: metamorphic characteristics and tectonic implications. In: Yoshida, M., Windley, B.F., Dasgupta, S. (Eds.), Proterozic East Gondwana: Supercontinent Assembly and Breakup. Special Publication, vol. 206. Geological Society of London, pp. 203–230.

Hart, S.R., Blusztajn, J., Craddock, C., 1995. Cenozoic volcanism in Antarctica — Jones Mountains and Peter-I Island. Geochimica et Cosmochimica Acta 59, 3379–3388.

Hart, S.R., Blusztain, J., LeMasurier, W.E., Rex, D.C., 1997. Hobbs Coast volcanism: implications for the West Antarctic rift system. Chemical Geology 139, 223–248.

Heaman, L.M., Kjarsgaard, B.A., Creaser, R.A., 2004. The temporal evolution of North American kimberlites. Lithos 76, 377–397.

Hill, P.J., Exon, N.F., 2004. Tectonics and basin development of the offshore Tasmanian area incorporating results from deep ocean drilling. The Cenozoic Southern Ocean: Tectonics, Sedimentation, and Climate Change between Australia and Antarctica. Geophysical Monograph Series, vol. 151. American Geophysical Union, Washington, D. C., pp. 19–142.

Hill, R.I., Campell, I.H., Davies, G.F., Griffiths, R.W., 1992. Mantle plumes and continental tectonics. Science 256, 186–193.

Hung, S.-H., Shen, Y., Ciao, L.-Y., 2004. Imagining seismic velocity structure beneath the Iceland hot spot: a finite frequency approach. Journal of Geophysical Research 109, B08305. doi:10.1029/2033JB002889.

Irvine, G.J., Pearson, D.G., Kjarsgaard, B.A., Carlson, R.W., Kopylova, M.G., Dreibus, G., 2003. A Re–Os isotope and PGE study of kimberlite-derived peridotite xenoliths from Somerset Island and a comparison to the Slave and Kaapvaal cratons. Lithos 71, 461–488.

Jellinek, A.M., Manga, M., 2004. Links between long-lived hot spots, mantle plumes, D″, and plate tectonics. Reviews of Geophysics 42, RG3002. doi:10.1029/2003RG000144.

Jordan, T.H., 1974. Some comments on tidal drag as a mechanism for driving plate motions. Journal of Geophysical Research 79, 2141–2142.

Ishii, M., Tromp, J., 2004. Constraining large-scale mantle heterogeneity using mantle and inner-core sensitive normal modes. Physics of the Earth and Planetary Interiors 146, 113–124.

Kaminski, E., Jaupart, C., 2000. Lithospheric structure beneath the Phanerozoic intracratonal basins of North America. Earth and Planetary Science Letters 178, 139–149.

Ke, V., Solomatov, V.S., 2004. Plume formation in strongly temperature-dependent viscosity fluid over a very hot surface. Physics of Fluids 16, 1059–1063.

Kellogg, L.H., Hager, B.H., van der Hilst, R.D., 1999. Compositional stratification in the deep mantle. Science 283, 1881–1884.

Kopp, H., Kopp, C., Phipps Morgan, J., Flueh, E.R., Weinrebe, W., Morgan, W.J., 2003. Fossil hot spot–ridge interaction in the Musicians seamount province: geophysical investigations of hotspot volcanism at volcanic elongated ridges. Journal of Geophysical Research 108. doi:10.1029/2002JB002015.

Kopylova, M.G., Lo, J., Christensen, N.L., 2004. Petrological constraints on seismic properties of the Slave upper mantle (Northern Canada). Lithos 77, 493–510.

Korenaga, J., 2005. Firm mantle plumes and the nature of the core–mantle boundary region. Earth and Planetary Science Letters 232, 29–37.

Labrosse, S., 2002. Hotspots, mantle plumes and core heat loss. Earth and Planetary Science Letters 199, 147–156.

Labrosse, S., 2003. Thermal and magnetic evolution of the Earth's core. Physics of the Earth and Planetary Interiors 140, 127–143.

Laio, A., Bernard, S., Chiarotti, G.L., Scandolo, S., Tosatti, E., 2000. Physics of iron at Earth's core conditions. Science 287, 1027–1030.

Lanyon, R., Varne, R., Crawford, A.J., 1993. Tasmanian Tertiary basalts, the Balleny plume, and opening of the Tasman Sea (southwest Pacific Ocean). Geology 21, 555–558.

Lay, T., Garnero, E.J., Williams, Q., 2004. Partial melting in a thermo-chemical boundary layer at the base of the mantle. Physics of the Earth and Planetary Interiors 146, 441–467.

Le Bars, M., Davaille, A., 2004. Whole layer convection in a heterogeneous planetary mantle. Journal of Geophysical Research 109, B03403. doi:10.1029/2003JB002617.

Lehtonen, M.L., O'Brien, H.E., Peltonen, P., Johanson, B.S., Pakkanen, L.K., 2004. Layered mantle at Karelian craton margin: P–T of mantle xenocryst and xenoliths from the Kaavi–Kuopio kimberlites, Finland. Lithos 77, 593–608.

Lei, J., Zhao, D., 2006. A new insight into the Hawaiian plume. Earth and Planetary Science Letters 241, 438–453.

LeMasurier, W.E., Thomson, J.W. (Eds.), 1990. Volcanoes of the Antarctic Plate and the Southern Oceans. Antarctic Research Series, vol. 48. American Geophysical Union, Washington, D.C., p. 487.

Lenardic, A., Moresi, L., 2003. Thermal convection below a conducting lid of variable extent: heat flow scalings and two-dimensional, infinite Prandtl number numerical simulations. Physics of Fluids 15, 455–466.

Lenardic, A., Moresi, L.-N., Mühlhaus, H., 2003. Longevity and stability of cratonic lithosphere: insights from numerical simulations of coupled mantle convection and continental tectonics. Journal of Geophysical Research 108. doi:10.1029/2002JB001859.

Lin, P.E., van Veken, S.-C., 2006. Dynamics of thermochemical plumes: 1. Plume formation and entrainment of a dense layer. Geochemistry Geophysics Geosystems 7. doi:10.1029/2005GC001071.

Lisker, F., Brown, R., Fabel, D., 2003. Denudation and thermal history along a transect across the Lambert Graben, northern Prince Charles Mountains, Antarctica, derived from apatite fission track thermochronology. Tectonics 22, 1005. doi:10.1029/2002TC001477.

Loper, D.E., Stacey, F.D., 1983. The dynamical and thermal structure of deep mantle plumes. Physics of the Earth and Planetary Interiors 33, 304–317.

Lythe, M.B., Vaughan, D.G., 2001. BEDMAP: a new ice thickness and subglacial topographic model of Antarctica. Journal of Geophysical Research 106, 11335–11351.

Macphail, M.K., Truswell, E.M., 2004. Palynology of Site 1166, Prydz Bay, East Antarctica. Proceedings of the Ocean Drilling Program 188, ms. # 188SR-013.

Masters, G., Gubbins, D., 2003. On the resolution of density within the Earth. Physics of the Earth and Planetary Interiors 140, 159–167.

McNamara, A.K., Zhong, S., 2004. Thermochemical structures within a spherical mantle: superplumes or piles? Journal of Geophysical Research 109, B07402. doi:10.1029/2003JB002847.

Meibom, A., Sleep, N.H., Zahnle, K., Anderson, D.L., 2005. Models for noble gases in mantle geochemistry: some observations and alternatives. In: Foulger, G.R., Natland, J.H., Presnall, D.C., Anderson, D.L. (Eds.), Plates, plumes, and paradigms. Geological Society of America Special Paper, vol. 388, pp. 347–363.

Mittelstaedt, E., Tackley, P.J., 2006. Plume heat flow is much lower than CMB heat flow. Earth and Planetary Science Letters 241, 202–210.

Montelli, R., Nolet, G., Dahlen, F.A., Masters, G., Engdahl, E.R., Hung, S.-H., 2004. Finite-frequency tomography reveals a variety of plumes in the mantle. Science 303, 338–343.

Mooney, W.D., Vidale, J.E., 2003. Thermal and chemical variations in subcrustal cratonic lithosphere: evidence from crustal isostasy. Lithos 71, 185–193.

Morelli, A., Danesi, S., 2004. Seismological imagining of the Antarctic continental lithosphere: a review. Global and Planetary Change 42, 155–165.

Morgan, W.J., 1972. Plate motions and deep convection. Geological Society of America Memoir 132, 7–22.

Morgan, W.J., 1978. Rodriguez, Darwin, Amsterdam, …, A second type of hotspot island. Journal of Geophysical Research 83, 5355–5360.

Müller, R.D., Cande, S.C., Stock, J.M., Keller, W.R., 2005. Crustal structure and rift flank uplift of the Adare Trough, Antarctica. Geochemistry Geophysics Geosystems 6, Q11010.

Nakagawa, T., Tackley, P.J., 2004a. Thermo-chemical structure in the mantle arising from a three-component convective system and implications for geochemistry. Physics of the Earth and Planetary Interiors 146, 125–138.

Nakagawa, T., Tackley, P.J., 2004b. Effects of a perovskite–post perovskite phase change near core–mantle boundary in compressible mantle convection. Geophysical Research Letters 31, L16611. doi:10.1029/2004GL020648.

Nardini, I., Armienti, P., Rocchi, S., Burgess, S., 2003. ^{40}Ar–^{39}Ar Chronology and petrology of the Miocene rift-related volcanism Daniell Peninsula (northern Victoria Land, Antarctica). Terra Antartica 10, 39–62.

Ni, A., Helmberger, D.V., 2003. Further constraints on the Africa superplume structure. Physics of the Earth and Planetary Interiors 140, 243–251.

Nimmo, F., Price, G.D., Brodholt, J., Gubbins, D., 2004. The influence of potassium on core and geodynamo evolution. Geophysical Journal International 156, 363–376.

Nyblade, A.A., Sleep, N.H., 2003. Long lasting epeirogenic uplift from mantle plumes and the origin of the southern African Plateau. Geochemistry Geophysics Geosystems 4, 1105. doi:10.1029/2003GC000573.

Olson, P., Schubert, G., Anderson, C., 1993. Structure of axisymmetric mantle plumes. Journal of Geophysical Research 98, 6829–6844.

O'Neill, C.J., Moresi, L., 2003. How long can diamonds remain stable in the continental lithosphere? Earth and Planetary Science Letters 213, 43–52.

Pearson, D.G., 1999. The age of continental roots. Lithos 48, 171–194.

Phillips, D., Harris, J.W., Vijoen, K.S., 2004. Mineral chemistry and thermobarometry from De Beers Pool diamonds, Kimberley South Africa. Lithos 77, 155–179.

Prestvik, T., Duncan, R.A., 1991. The geology and age of Peter I Oy, Antarctica. Polar Research 9, 89–98.

Price, G.D., Alfè, D., Vocadlo, L., Gillan, M.J., 2004. The Earth's core: an approach from first principles. In: Sparks, R.S.J., Hawkesworth, C.J. (Eds.), The State of the Planet, Frontiers and Challenges in Geophysics. Geophysical Monograph Series, vol. 150. American Geophysical Union, Washington D.C., pp. 1–12.

Putirka, K.D., 2005. Mantle potential temperatures at Hawaii, Iceland, and the mid-ocean ridge system, as inferred from olivine phenocrysts: evidence for thermally driven mantle plumes. Geochemistry Geophysics Geosystems 6, Q05L08.

Quilty, P.G., 1997. Eocene and younger biostratigraphy and lithofacies of the Cascade seamount, East Tasman Plateau, southwest Pacific Ocean. Australian Journal of Earth Sciences 44, 655–665.

Ranalli, G., 2000. Westward drift of the lithosphere: not a result of rotational drag. Geophysical Journal International 141, 535–537.

Read, G., Grutter, H., Winter, S., Luckman, N., Gaunt, F., Thomsen, F., 2004. Stratigraphic relations, kimberlite emplacement and lithospheric thermal evolution. Quiricó basin, Minas Gerais State. Brazil. Lithos 77, 803–818.

Ricard, Y., Doglioni, C., Sabadini, R., 1991. Differential rotation between lithosphere and mantle: a consequence of lateral mantle viscosity variations. Journal of Geophysical Research 96, 8407–8415.

Richards, M.A., Griffiths, R.W., 1989. Thermal entrainment by deflected mantle plumes. Nature 342, 900–902.

Richards, M.A., Hager, B.H., Sleep, N.H., 1988. Dynamically supported geoid highs and hotspots: observation and theory. Journal of Geophysical Research 93, 7690–7708.

Richards, M.A., Ricard, Y., Lithgow-Bertelloni, C., Spada, G., Sabadini, R., 1997. An explanation for Earth's long-term rotational stability. Science 275, 372–375.

Richards, M.A., Yang, W.S., Baumgardner, J.R., Bunge, H.P., 2001. Role of a low-viscosity zone in stabilizing plate tectonics: implications for comparative terrestrial planetology. Geochemistry Geophysics Geosystems 2 2000GC000115.

Ritzwoller, M.H., Shapiro, N.M., Levshin, A.L., Leahy, G.M., 2001. Crustal and upper mantle structure beneath Antarctica and surrounding oceans. Journal of Geophysical Research 106, 30645–30670.

Rocchi, S., Armienti, P., D'Orazio, M., Tonarini, S., Wijbrans, J.R., Di Vincenzo, G., 2002a. Cenozoic magmatism in the western Ross Embayment: role of mantle plume versus plate dynamics in the development of the West Antarctic Rift System. Journal of Geophysical Research 107, 2195. doi:10.1029/JB0005155.

Rocchi, S., Fioretti, A.M., Cavzzine, G., 2002b. Petrography, geochemistry, and geochronology of the Cenozoic Cape Crossfire, Cape King, and No Ridge igneous complexes (northern Victoria, Land Antarctica). Antarctica at the close of a millennium. Royal Society of New Zealand Bulletin, vol. 35, pp. 215–225.

Rocchi, S., Armienti, P., Di Vincenzo, G., 2005. No, plume, no rift magmatism in the West Antarctic Rift. In: Foulger, G.R., Natland, J.H., Presnall, D.C., Anderson, D.L. (Eds.), Plates, Plumes, and Paradigms: Geological Society of America Special Paper, vol. 388, pp. 435–447.

Rowell, A.J., Van Schmus, W.R., Sorey, B.C., Fetter, A.H., Evans, K.R., 2001. Latest Neoproterozoic to Mid-Cambrian age for the main deformation phases of the Transantarctic Mountains: new stratigraphic and isotopic constraints from the Pensacola Mountains, Antarctica. Journal of the Geological Society 158, 295–308.

Royer, J.-Y., Rollet, N., 1997. Plate-tectonic setting of the Tasmanian region. Australian Journal of Earth Sciences 44, 543–560.

Rudnick, R.L., Nyblade, A.A., 1999. The thickness and heat production of Archean lithosphere: constraints from xenolith thermobarometry and surface heat flow. In: Fei, Y., Bertka, C.M., Mysen, B.O. (Eds.), Mantle Petrology: Field Observations and High Pressure Experimentation: A Tribute to Francis R. (Joe) Boyd. Geological Society, Special Publication, vol. 6, pp. 3–12.

Saltzer, R.L., Chatterjee, N., Grove, T.L., 2001. The spatial distribution of garnets and pyroxenes in mantle peridotites: pressure–temperature history of peridotites from the Kaapvaal craton. Journal of Petrology 42, 2215–2229.

Salvioli-Maiani, E., Toscani, L., Bersani, D., 2004. Magmatic evolution of the Gaussberg lamprolite (Antarctica): volatile content and glass composition. Mineralogical Magazine 68, 83–100.

Sandwell, D.T., Smith, W.H.F., 1997. Marine gravity anomaly from Geosat and ERS1 satellite altimetry. Journal of Geophysical Research 102, 10039–10054.

Schilling, J.G., 1991. Fluxes and excess temperatures of mantle plumes inferred from their interaction with migrating midocean ridges. Nature 352, 397–403.

Schimmel, M., Assumpção, M., VanDecar, J.C., 2003. Seismic velocity anomalies beneath SE Brazil from P and S wave travel time inversions. Journal of Geophysical 108. doi:10.1029/2001JB000187.

Schmidberger, S.S., Simonetti, A., Francis, D., Gariepy, C., 2002. Probing Archean lithosphere using the Lu–Hf isotope systematics of periodite xenoliths from Somerset Island kimberlites, Canada. Earth and Planetary Science Letters 197, 245–259.

Schubert, G., Matser, G., Olson, P., Tackley, P., 2004. Superplumes or plume clusters. Physics of the Earth and Planetary Interiors 146, 147–162.

Schulze, D.J, Harte, B., Valley, J.W., Brenan, J.M., Channer, D.M. de R., 2003a. Extreme crustal oxygen isotope signatures preserved in coesite in diamond. Nature 423, 68–70.

Schulze, D.J., Valley, J.W., Spicuzza, M.J., Channer, D.M. de R., 2003b. The oxygen isotope composition of eclogitic and peridotitic garnet xenoliths from the La Ceniza kimberlite, Guaniamo, Venezuela. International Geology Review 45, 968–975.

Schulze, D.J., Harte, B., Valley, J.W., Channer, D.M. de R., 2004. Evidence of subduction and crust–mantle mixing from a single diamond. Lithos 77, 349–358.

Scoppola, B., Boccaletti, D., Bevis, M., Carminati, E., Doglioni, C., 2006. The westward drift of the lithosphere: a rotational

drag? Geological Society of America Bulletin 118, 199–209. doi:10.1130/B25734.1.
Sengör, A.M.C., Natal'in, B.A., 2001. Rifts of the World. In: Ernst, R. E., Buchan, K.L. (Eds.), Mantle Plumes: Their Identification through Time: Boulder Colorado. Geological Society of America Special Paper, vol. 352, pp. 389–482.
Shapiro, N.M., Ritzwoller, M.H., 2004. Inferring surface heat flux distributions guided by a global seismic model: particular application to Antarctica. Earth and Planetary Science Letters 223, 213–224.
Shapiro, S.S., Hager, B.H., Jordan, T.H., 1999a. The continental tectosphere and Earth's long-wavelength gravity field. Lithos 48, 135–152.
Shapiro, S.S., Hager, B.H., Jordan, T.H., 1999b. Stability and dynamics of the continental tectosphere. Lithos 48, 115–133.
Shaw, H.R., Jackson, E.D., 1973. Linear island chains in the Pacific, result of thermal plumes or gravitational anchors? Journal of Geophysical Research 78, 8634–8652.
Sheraton, J.W., 1983. Geochemistry of mafic igneous rocks of the northern Prince Charles Mountains, Antarctica. Journal of the Geological Society of Australia 30, 295–304.
Shirey, S.B., Harris, J.W., Richardson, S.H., Fouch, M., James, D.E., Cartigny, P., Deines, P., Viljoen, F., 2003. Regional patterns in the paragenesis and age of inclusion in diamond, diamond composition, and the lithospheric seismic structure of Southern Africa. Lithos 71, 243–258.
Shirey, S.B., Richardson, S.H., Harris, J.W., 2004. Integrated models of diamond formation and craton evolution. Lithos 77, 923–944.
Sieminski, A., DeBayle, E., Levêque, J.-J., 2003. Seismic evidence for deep low-velocity anomalies in the transition zone beneath West Antarctica. Earth and Planetary Science Letters 216, 645–661.
Sleep, N.H., 1988. Gradual entrainment of a chemical layer at the base of the mantle by overlying convection. Geophysical Journal 95, 437–447.
Sleep, N.H., 1990a. Hotspots and mantle plumes: some phenomenology. Journal of Geophysical Research 95, 6715–6736.
Sleep, N.H., 1990b. Monteregian hotspot track: a long-lived mantle plume. Journal of Geophysical Research 95, 21983–21990.
Sleep, N.H., 2002. Ridge-crossing mantle plumes and gaps in tracks. Geochemistry Geophysics Geosystems 3. doi:10.1029/2001GC000290.
Sleep, N.H., 2003a. Geodynamic implications of xenolith geotherms. Geochemistry Geophysics Geosystems 4, 1079. doi:10.1029/2003GC000511.
Sleep, N.H., 2003b. Survival of Archean cratonal lithosphere. Journal of Geophysical 108. doi:10.1029/2001JB000169.
Sleep, N.H., 2003c. Fate of mantle plume material trapped within a lithospheric catchment with reference to Brazil. Geochemistry Geophysics Geosystems 4. doi:10.1029/2002GC000464.
Sleep, N.H., 2004. Thermal haloes around plume tails. Geophysical Journal International 156, 359–362.
Solomatov, V.S., 1995. Scaling of temperature- and stress-dependent viscosity convection. Physics of Fluids 7, 266–274.
Solomatov, V.S., Moresi, L.-N., 2000. Scaling of time-dependent stagnant lid convection: application to small-scale convection on Earth and other terrestrial planets. Journal of Geophysical Research 105, 21795–21817.
Solomatov, V.S., Moresi, L.-N., 2002. Small-scale convection in the D″ layer. Journal of Geophysical Research 107. doi:10.1029/2000JB000063.
Steinberger, B., 2000. Plumes in a convecting mantle: models and observations for individual hotspots. Journal of Geophysical Research 105, 11127–11152.
Steinberger, B., Sutherland, R., O'Connell, R.J., 2004. Prediction of Emperor–Hawaii seamount locations from a revised model of global plate motion and mantle flow. Nature 430, 167–173.
Stock, J.M., Cande, S.C., 2002. Tectonic history of Antarctic seafloor in the Australia–New Zealand–South Pacific sector: implications for Antarctic continental tectonics. Antarctica at the close of a millennium. Royal Society of New Zealand Bulletin, vol. 35, pp. 251–259.
Storey, B.C., Leat, P.T., Weaver, S.D., Pankhurst, R.J., Bradshaw, J.D., Kelley, S., 1999. Mantle plumes and Antarctic–New Zealand rifting: evidence from mid-Cretaceous mafic dykes. Journal of the Geological Society 156, 659–671.
Strand, K., Passchier, S., Näsi, J., 2003. Implications of quartz grain microtextures for onset of Eocene/Oligocene glaciation in Prydz Bay, ODP Site 1166, Antarctica. Paleogeography, Paleoclimatology, Paleoecology 198, 101–111.
Studinger, M., Karner, G.B., Bell, R.E., Levin, V., Raymond, C.A., Tikku, A.A., 2003. Geophysical models for the tectonic framework of the Lake Vostok region, East Antarctica. Earth and Planetary Science Letters 216, 663–677.
Taylor, J., Siegert, M.J., Payne, A.J., Hambrey, M.J., Cooper, P.E., Leitchenkov, A.K., 2004. Topographic controls on post-Oligocene changes in ice-sheet dynamics, Prydz Bay region, East Antarctica. Geology 32, 197–200.
Thorne, M.S., Garnero, E.J., Grand, S.P., 2004. Geographic correlation between hot spots and deep mantle lateral shear–wave velocity gradients. Physics of the Earth and Planetary Interiors 146, 47–63.
Tingey, R.J., McDougall, I., Gleadow, A.J.W., 1983. The age and mode of formation of Gaussberg, Antarctica. Journal of the Geological Society of Australia 30, 241–246.
Udintsev, G.B., Gersonde, R., Teterin, D.E., Schenke, G.W., Beresnev, A.F., Gohl, K., Titaeva, N.A., Fenogenov, A.N., Kurentsova, N.A., Roshchina, I.A., 2002. Peter I Island, Pacific Ocean, western Antarctica. Doklady Earth Sciences 386, 821–826 (English translation from Russian).
van den Berg, A.P., Yuen, D.A., Allwardt, J.R., 2002. Non-linear effects from variable thermal conductivity and mantle internal heating: implications for massive melting and secular cooling of the mantle. Physics of the Earth and Planetary Interiors 129, 359–375.
van der Hilst, R.D., de Hoop, M.V., 2005. Banana–doughnut kernels and mantle tomography. Geophysical Journal International 163, 956–961.
Wang, C.G., 1975. Are continents adrift, or driven? New Asia College Academic Annual 17, 347–354.
Weertman, J., Blacic, J., 1984. Harper–Dorn creep: an artifact of low-amplitude temperature cycling? Geophysical Research Letters 11, 117–120.
Whitehead, J.A., 1982. Instabilities of fluid conduits in a flowing Earth —are plates lubricated by the asthenosphere? Geophysical Journal of the Royal Astronomical Society 70, 415–433.
Wilson, J.T., 1963. Possible origin of Hawaii islands. Canadian Journal of Physics 41, 863–870.
Winberry, J.P., Anandaknishnan, S., 2004. Crustal structure of the West Antarctic rift system and Marie Byrd Land hotspot. Geology 32, 977–980.
Wysoczanski, R.J., Allibone, A.H., 2004. Age, correlation, and provenance of the Neoproterozoic Skelton Group, Antarctica: Grenville age detritus on the margin of East Antarctica. Journal of Geology 112, 401–416.